Evaluating aerosol/cloud/radiation process parameterizations with single-column models and Second Aerosol Characterization Experiment (ACE-2) cloudy column observations

Surabi Menon,[1,2,3] Jean-Louis Brenguier,[4] Olivier Boucher,[5] Paul Davison,[6,7] Anthony D. Del Genio,[1] Johann Feichter,[8] Steven Ghan,[9] Sarah Guibert,[4] Xiaohong Liu,[10] Ulrike Lohmann,[11] Hanna Pawlowska,[12] Joyce E. Penner,[10] Johannes Quaas,[13] David L. Roberts,[6] Lothar Schüller,[14] and Jefferson Snider[15]

[1]   The Second Aerosol Characterization Experiment (ACE-2) data set along with ECMWF reanalysis meteorological fields provided the basis for the single column model (SCM) simulations, performed as part of the PACE (Parameterization of the Aerosol Indirect Climatic Effect) project. Six different SCMs were used to simulate ACE-2 case studies of clean and polluted cloudy boundary layers, with the objective being to identify limitations of the aerosol/cloud/radiation interaction schemes within the range of uncertainty in in situ, reanalysis and satellite retrieved data. The exercise proceeds in three steps. First, SCMs are configured with the same fine vertical resolution as the ACE-2 in situ data base to evaluate the numerical schemes for prediction of aerosol activation, radiative transfer and precipitation formation. Second, the same test is performed at the coarser vertical resolution of GCMs to evaluate its impact on the performance of the parameterizations. Finally, SCMs are run for a 24–48 hr period to examine predictions of boundary layer clouds when initialized with large-scale meteorological fields. Several schemes were tested for the prediction of cloud droplet number concentration (N). Physically based activation schemes using vertical velocity show noticeable discrepancies compared to empirical schemes due to biases in the diagnosed cloud base vertical velocity. Prognostic schemes exhibit a larger variability than the diagnostic ones, due to a coupling between aerosol activation and drizzle scavenging in the calculation of N. When SCMs are initialized at a fine vertical resolution with locally observed vertical profiles of liquid water, predicted optical properties are comparable to observations. Predictions however degrade at coarser vertical resolution and are more sensitive to the mean liquid water path than to its spatial heterogeneity. Predicted precipitation fluxes are severely underestimated and improve when accounting for sub-grid liquid water variability. Results from the 24–48 hr runs suggest that most models have problems in simulating boundary layer cloud morphology, since the large-scale initialization fields do not accurately reproduce observed meteorological conditions. As a result, models significantly overestimate optical properties. Improved cloud morphologies were obtained for models with subgrid inversions and subgrid cloud thickness schemes. This may be a result of representing subgrid scale effects though we do not rule out the possibility that better large-forcing data may also improve cloud morphology predictions.   *INDEX TERMS:* 0305 Atmospheric Composition and Structure: Aerosols and particles (0345, 4801); 0320 Atmospheric Composition

---

[1]NASA Goddard Institute for Space Studies, New York, USA.

[2]Center for Climate Systems Research, Columbia University, New York, USA.

[3]Also at EETD, Lawrence Berkeley National Laboratory, Berkeley, California, USA.

[4]Météo-France-CNRS, CNRM-GAME, Toulouse, France.

[5]Laboratoire d'Optique Atmosphérique, Universitédes Sciences et Technologies de Lille, Villeneuve d'Ascq, France.

[6]Hadley Centre, Met Office, Exeter, UK.

[7]Now at Environment Systems Group, ADS, Wolverhampton, UK.

[8]Max Planck Institute for Meteorology, Hamburg, Germany.

[9]Climate Physics Group, Pacific Northwest National Laboratory, Richland, Washington, USA.

[10]Department of Atmospheric, Oceanic and Space Sciences, University of Michigan, Ann Arbor, Michigan, USA.

[11]Department of Physics and Atmospheric Science, Dalhousie University, Halifax, Canada.

[12]Institute of Physics, Warsaw University, Warsaw, Poland.

[13]Laboratoire de Météorologie Dynamique/CNRS, Paris, France.

[14]Institut für Weltraumwissenschaften, Freie Universität, Berlin, Germany.

[15]Department of Atmospheric Science, University of Wyoming, Laramie, Wyoming, USA.

and Structure: Cloud physics and chemistry; 3354 Meteorology and Atmospheric Dynamics: Precipitation (1854); 3359 Meteorology and Atmospheric Dynamics: Radiative processes; *KEYWORDS:* aerosol indirect effect, cloud microphysics, cloud optics

1. Introduction

[2] The aerosol/cloud/radiation interaction process, referred to as the aerosol indirect effect (AIE), is estimated to be highly uncertain but potentially large enough ($\sim$0 to -4.8 W m^{-2}) [*Penner et al.*, 2001] to counteract part of the greenhouse warming. For models that treat aerosol effects on all types of clouds, the contributions to the AIE from low-level stratiform clouds are quite important. First their moderate albedo is more sensitive to cloud microphysics modifications than deep, highly reflective clouds (first indirect effect) [*Twomey*, 1977]. Second their moderate geometrical thickness is often just sufficient for cloud droplets to reach a precipitating size. A slight increase in cloud droplet number concentration (N) is therefore likely to prevent the onset of precipitation, affecting the cloud liquid water path (LWP) and cloud cover (second indirect effect) [*Albrecht*, 1989].

[3] Models predict N via either a diagnostic or prognostic scheme. In prognostic schemes N refers to the droplet concentration predicted from the balance between droplet production by activation of the aerosols and droplet scavenging by precipitating drops. Diagnostic schemes can be based on either empirical relationships between aerosol mass/number concentration (N_a) and N (thus implicitly accounting for droplet scavenging, unless drizzle conditions are filtered from the training data base), or on the same mechanistic relationships between N_a and N [*Abdul-Razzak and Ghan*, 2000] that are used to treat activation in prognostic schemes (thus neglecting the influence of droplet scavenging). These schemes reflect conceptual ambiguities in the definition of N in a GCM. A common approach is to define N as the spatial average of the local values of droplet concentration over the cloud fraction of a GCM grid. It is difficult however to derive such a mean value from the initial value predicted with an aerosol activation scheme [*Zhang et al.*, 2002], without subgrid information on mixing with the environmental air and scavenging by precipitation, both leading to a diminution of the initial value. Here, a different approach was employed in the processing of the Second Aerosol Characterization Experiment (ACE-2) data set that is used for validation of the parameterizations. Each case study has been characterized by a value of N representative of the activation process, before diminution by mixing and scavenging [*Pawlowska and Brenguier*, 2003]. Cloud radiative properties [*Schüller et al.*, 2003] and the precipitation cycle [*Pawlowska and Brenguier*, 2003] have both been examined in relation to these activation-representative values of N.

[4] The treatment of the second AIE in models with parameterized microphysics is through the auto-conversion (Qaut) scheme (self collection of cloud drops), that links N with the onset of precipitation, and the accretion scheme (collection of cloud drops by raindrops), that together with auto-conversion determines the production of precipitation. Since most GCMs do not account for subgrid liquid water content (LWC) variability in these schemes, this has implications not only for the computed Qaut rates but also for cloud radiative properties. (Models with bin resolved microphysics avoid these problems since they do not use the Qaut and accretion schemes, but the need to parameterize cloud-scale vertical velocities remains a major problem when determining updraft effects on cloud microphysical variables). This variability in LWC is thought to have a larger impact on the mesoscale average albedo than the usual cloud fraction corrections [*Cahalan*, 1994]. Furthermore, satellite records of cloud radiative properties indicate that much of the cloud optical depth variability is due to LWP variability [*Schwartz et al.*, 2002] and that polluted air masses have warmer cloud temperatures and thinner clouds [*Harshvardhan et al.*, 2002]. The ACE-2 data base of 8 case studies corroborates these satellite observations, with polluted cloud systems that are thinner than the marine cases, attributed to their continental origin [*Brenguier et al.*, 2003]. Thus to discern aerosol influences on clouds, besides meteorological influences, variability in cloud thickness and LWC are equally important.

[5] To account for the inability of a GCM with a coarse vertical resolution to explicitly resolve clouds, and to narrow the uncertainty associated with the aerosol/cloud/radiation process parameterizations, we present results from simulations carried out with single column models (SCM) that represent a single grid column of the parent GCM. The effects of large-scale dynamics are important when simulating the indirect effect and as yet there are no global scale observations that enable a separation of synoptic effects from aerosol effects on clouds. Thus the comparison and evaluation of different schemes commonly employed in GCMs for the AIE are easier to accomplish using a SCM, since there are fewer dynamical differences between models and known dynamical changes can be isolated, assuming that all SCMs start with the same dynamical setting. The data set used to initialize and constrain model results is from the ACE-2 Cloudy Column (CC) Project held in Tenerife in 1997. The results of this project are described in *Brenguier et al.* [2000a, 2000b, 2003], *Guibert et al.* [2003], *Pawlowska and Brenguier* [2003], *Schüller et al.* [2003], *Snider et al.* [2003], and *Zhang et al.* [2002].

[6] Here, we use observed profiles of temperature, humidity, large-scale forcing fields and aerosol properties, to see if the SCMs can differentiate between cloud properties observed in clean versus polluted air masses during the ACE-2 CC Project? Six different SCMs were used in this study and the differences between SCM simulations and observations of relevant cloud fields, if isolated, could

provide some guidance on the needed accuracy and type of parameterizations required to simulate processes critical to the AIE.

2. Data Description

2.1. Cloudy Column Data

[7] Submicron aerosol mass data used for the prediction of N were collected at a surface site located on the northeastern coast of Tenerife, at the top of the Punta Del Hidalgo (PDH) lighthouse that is ∼50 m above sealevel [*Putaud et al.*, 2000]. Non sea-salt sulfate was the dominant aerosol type. In situ data were collected on board the Meteo-France instrumented aircraft Merlin-IV that flew along a square track with a horizontal dimension of 60 km, either at a constant altitude in cloud or below cloud base, or ascending and descending from above to below the cloud layer [*Brenguier et al.*, 2000b]. Aerosol number concentrations, in particular N_a (derived using size spectra measurements for particles larger than 0.1 μm from the PDH site), and updraft velocity statistics (from aircraft measurements), that are required for parameterizations of the aerosol activation process, are described by *Guibert et al.* [2003] and *Snider et al.* [2003]. Layer data for cloud dynamical and microphysical properties are in *Brenguier et al.* [2003]. According to the data processing method described in *Pawlowska and Brenguier* [2003], N is the mean value of the frequency distribution of the measured droplet concentration after selection of cloud samples that are not affected by either mixing or drizzle scavenging; hence N aims at reflecting the impact of aerosols on cloud microphysics, irrespective of further diminution processes. That value of N is larger than the mean value over the whole cloud layer, as indicated by *Pawlowska and Brenguier* [2000, Figures 2 and 3] for the June 25 (70 against 53 cm^{-3}) and July 9 (244 against 173 cm^{-3}) cases respectively. The small difference between N values used in this paper and those by *Pawlowska and Brenguier* [2000]: (75 against 70 cm^{-3} for the June 25 case, and 256 against 244 cm^{-3} for July 9) is explained in *Pawlowska and Brenguier* [2003]. A maximum mean volume droplet radius (MVDR) was also derived, such that 98% of the sampled droplet spectra exhibit MVDR values smaller than the indicated value. The difference between MVDR and effective radius values (∼1 μm) was lower than the difference between the various radiative transfer schemes, using either the vertical mean effective radius, the effective radius at cloud top, or the effective radius five optical thickness units below cloud top and are based on methodologies discussed by *Brenguier et al.* [2000a, 2000b]. Thus the maximum MVDR was used as a surrogate for the effective radius at cloud top that determines the cloud radiative properties as well as the likelihood for droplets to grow above the auto-conversion critical radius for the onset of precipitation. Such a maximum droplet size however is not commonly predicted in GCM parameterizations that rather consider its mean value averaged horizontally over the cloudy fraction of a grid and vertically over the cloud layer thickness. In this paper, we therefore also use a mean value of the observed MVDR, averaged over all cloudy samples. The cloud geometrical thickness H is derived in *Pawlowska and Brenguier* [2003] such that 98% of the cloudy samples are measured at an altitude above cloud base smaller than the indicated value. Adiabatic predictions of LWC and of layer mean MVDR were calculated for each case as functions of N and H.

[8] Independent estimations of N, H, LWP, cloud optical depth, cloud albedo and broadband albedo (200 nm to 5000 nm) were derived from the multispectral radiance measurements with the radiometer OVID, operated on board the DLR-Do-228 aircraft flying about 1 km above cloud top, with the retrieval techniques of *Schüller et al.* [2003]. The retrieved cloud optical depth and cloud albedo were calculated over the cloudy fraction of the square pattern, while the broadband albedo was derived for the whole area (cloudy and cloud free). Retrievals of N, H and LWP from OVID radiances are based on the assumption of an adiabatic LWC vertical profile in the cloud layer. N is retrieved from the 10% most reflective samples in order to characterize the undiminished cloud regions, as was the case for the in situ derived value. In contrast, the frequency distributions of H and LWP are retrieved from the 90% most reflective samples (the remaining 10% are classified as cloud free samples) and thus they illustrate the variability of the whole cloud layer. Cloud fraction (portion of sky covered with clouds in a pixel) was estimated from the compact airborne spectrographic imager (CASI) [*Schröder et al.*, 2002] that has a spatial resolution of 4 m across track and 15 m along track. Most of these measurements were time averaged over the observation period, limited to 3–4 hours around noon local time. Therefore we also use additional measurements from the International Satellite Cloud Climatology Project (ISCCP) [*Rossow and Schiffer*, 1991].

2.2. Cloudy Column Cases

[9] The complete data set from the CC experiment consists of 8 cases described by *Brenguier et al.* [2000a]. In Table 1 we list the values of the key variables obtained from the CC experiment for 5 of the 8 cases: 2 marine (June 25 and 26) and 3 polluted cases (July 8, 9 and 18). The other 3 cases were a mix of polluted and marine air masses and are not evaluated in this study. As can be seen, the marine cases are characterized by smaller aerosol mass, N_a, and N, and larger droplet size, cloud thickness and mean LWC than the polluted cases. It can also be noticed that the radiative properties are dependent on both H and N. For example between June 25 and July 9, N increases by a factor of 3.4, while H decreases slightly. The larger thickness on June 25 (262 m) compared to July 9 (167 m) in fact compensates for the effect of increasing N. The respective contributions of N and H to cloud radiative properties during ACE-2 are examined by *Brenguier et al.* [2003]. Thus it is the dynamical setting that may also influence the radiative properties of the cloud and hence the indirect effect, in addition to the change in aerosol.

[10] To further understand the modifications to cloud radiative properties that result from the difference in aerosol and cloud microphysical properties, we shall mainly focus on the marine case of June 26 and the polluted case of July 9, since from all the cases shown in Table 1, June 26 and July 9 have the largest contrast in N and cloud drop radius, (an increase by a factor of 5 for N and a 40% decrease in cloud drop radius for July 9). The general meteorological conditions during ACE-2 are in the work of *Raes et al.* [2000], and the meteorological conditions

Table 1. Mean Values of the Microphysical and Radiative Properties of Five of the Cloudy Column Cases[a]

Date	Aerosol Mass, $\mu g\ m^{-3}$	N_a, cm^{-3}	N, cm^{-3}	r_v, μm	LWC, $g\ m^{-3}$	LWP, $g\ m^{-2}$	Cloud Thickness, m	Cloud Optical Depth	Cloud Albedo
25 June	0.7	225	75 ± 16	7.31 ± 3.67	0.137 ± 0.11	26.0 ± 24.5	262	5.86 ± 3.28	0.25 ± 0.04
26 June	1.2	215	52 ± 16	7.77 ± 3.64	0.125 ± 0.097	18.5 ± 17.8	202	3.99 ± 2.29	0.19 ± 0.03
8 July	7.2	588	208 ± 31	5.36 ± 1.57	0.128 ± 0.10	18.7 ± 14.5	182	5.86 ± 3.12	0.29 ± 0.04
9 July	5.8	575	256 ± 38	4.73 ± 1.67	0.110 ± 0.083	11.0 ± 10.8	167	4.23 ± 2.54	0.27 ± 0.04
18 July	5.9	869	178 ± 40	5.24 ± 2.03	0.116 ± 0.108	15.7 ± 17.6	192	4.92 ± 3.14	0.28 ± 0.04

[a]Aerosol mass refers to the total mass of all submicrometric particles (nitrate, nss sulfate, sea-salt, organic and black carbon, ammonium and dust) and N_a refers to aerosol concentration (or condensation nuclei count). N, r_v, LWC, LWP refer to the cloud droplet number concentration, mean volume droplet radius and liquid water content averaged over the cloud layer, and liquid water path of the cloud as obtained from the Fast FSSP measurements. (Note that LWP values are derived from a maximum overlap model that uses measured LWC profiles). Cloud optical depth values are from extinction measurements (also from the Fast FSSP measurements and maximum overlap model) and cloud albedos are from OVID retrievals.

prior to the cloud formation for these events [*Verver et al.*, 2000] are briefly described.

[11] During the period of June 25 through July 3 a cyclone was present over western Europe bringing in clean maritime air over the ACE-2 area; the cyclone subsequently weakened and disappeared by the 3rd and 4th of July. A high pressure ridge then developed and covered most of the North Atlantic region from the 4th until the 10th of July. These 2 synoptic events led to the clean and polluted cases observed during the CC campaign described in Table 1. *Verver et al.* further found that the position of the Azores high usually determined the outflow of pollution from Europe to the ACE-2 region. Back-trajectory analysis of the air masses in *Verver et al.* confirm the maritime and continental origin of the air masses that led to the June 26 and July 9 cases, respectively. Large-scale vertical velocity fields obtained from European Centre for Medium-Range Weather Forecasts (ECMWF) reanalysis for these 2 cases indicate increased subsidence for the July 9 case. Thus the synoptic evolution of these 2 cases and the origin of the air masses, suggest that the cloud forming air mass for the June 26 case was thicker and had more moisture than the July 9 case as indicated by the values shown in Table 1. In addition, evaluation of the 24 hour cycle of the observed cloud (with ISCCP retrieved data) for the June 26 event indicates a diurnal cycle similar to that of marine strato-cumulus clouds observed during the Atlantic Strato-cumulus Experiment (ASTEX) [*Albrecht et al.*, 1995]. In contrast, the lack of a diurnal cycle for July 9 (developed due to presence of a high pressure ridge) suggests that meteorological factors control the cloud evolution (as also indicated by the stronger sea level pressure changes within the 24 hour period than for June 26), and thus the diurnal variations of the cloud cycle are masked by the dynamics.

2.3. European Centre for Medium-Range Weather Forecasts (ECMWF) Reanalysis Data

[12] The simulation domain (2.5° × 2.5°) comprises four ECMWF columns whose centers are closest to the CC flight area, at 29.4N and 16.7W. Surface input variables include pressure, surface air temperature, sea surface temperature, sensible and latent heat fluxes; layer input variables include temperature (T), specific humidity (q_v), u and v components of wind, and vertical velocity. Six hourly data at the 31 ECMWF levels are interpolated to the time steps and levels used in the individual SCMs. The horizontal advective tendencies of T and q_v used to force the SCMs are calculated from products of the average wind and gradient across the four columns and are either set to zero with the assumption that horizontal drift is negligible for simulations <48 hours, or are set to values calculated from the ECMWF reanalysis. Vertical advections are calculated using the large-scale vertical velocity (from ECMWF reanalysis) and the SCM T or q_v profiles. Surface turbulent fluxes are calculated using the SCM parameterizations. A nudging term, when applied, is calculated as the difference between observations and SCM simulations for T or q_v divided by a nudging timescale, obtained from the advective timescale $\Delta x/v$, where v is the wind speed and Δx is the SCM grid size domain [*Ghan et al.*, 1999]. This nudging term is added to the forcing term. Nudging the T and q_v profiles can reduce errors from large-scale forcing but may mask errors from model physics, only if those errors impact temperature and humidity [*Ghan et al.*, 1999]. In general, nudging may introduce some discrepancy in cloud morphology since it could influence radiative heating and condensation processes by eliminating radiative feedback on cloud formation (W. B. Rossow, personal communication, 2002). However, nudging does not influence droplet activation processes that are of interest in this study since none of the models derive supersaturation from the simulated large-scale humidity and temperature. Additionally, since nudging has little influence on the updrafts (which are typically related to the simulated turbulence) or on the aerosol, it has little influence on supersaturation.

2.4. Consistency Between Observations and ECMWF Data

[13] To compare model products with observations, in situ measurements (cloud base and top, T and q_v soundings, aerosol mass, N, cloud droplet size, cloud optical depth, LWC, LWP); aircraft remote sensing retrieved data (LWP, cloud optical depth, cloud and planetary albedos); ECMWF reanalysis products (T and q_v soundings); and satellite retrieved data (cloud fraction, cloud top) are available. However, the disagreement between the estimates for LWP and cloud optical depth; and cloud base and top (Section 5.2.1) from in situ, reanalysis and remotely retrieved data were difficult to reconcile and hence are used as an indication of the range of uncertainty to constrain model products.

[14] For model validation of LWP and cloud optical depth, two sets of data are available -from in situ measurements, and from cloud remote sensing. They show noticable

discrepancies that are discussed in detail by *Schüller et al.* [2003] and *Brenguier et al.* [2003]. Their conclusions are briefly summarized here. In situ measurements of the droplet size distribution were used to derive LWC and the extinction coefficient. The numerous aircraft traverses from cloud base to top were used to derive vertically integrated parameters, such as optical thickness and LWP, by assuming either random or maximum overlap of the extinction and LWC frequency distributions. Remote sensing measurements of cloud top radiances in the visible and near infrared are used for the retrieval of cloud optical thickness and droplet effective radius. N and LWP were then derived from these retrievals based on the assumption of an adiabatic vertical distribution of LWC. The frequency distribution of the directly retrieved optical thickness agrees with the estimates derived from in situ measurements, assuming either random or maximum overlap. In contrast, the retrieved LWP frequency distribution departs substantially from that based on the in situ measurements and this discrepancy is attributed to the adiabatic assumption. However for both data sets the LWP frequency distributions exhibit similar tendencies, with a larger mean and standard deviation on June 26, compared to July 9.

3. Model Description

[15] Six different SCMs are used to evaluate the aerosol/cloud/radiation interaction parameterizations, abbreviated as CSIRO, GISS, MetO, PNNL, ECHAM and LMD. A brief description of the models is in Appendix A and the standard schemes used for cloud droplet nucleation and Qaut are in Table 2. All SCMs are run in a single column mode except for ECHAM and LMD that use a 3-D GCM nudged mode to run the SCM. In addition, the LMD also ran simulations using the simulated sulfate aerosol mass (Section 5.2.2) that allows it to evaluate the sulfate concentrations with those observed and the corresponding effect on N.

[16] The key differences among the models in the context of this study are those that use a prognostic treatment for cloud droplet activation (PNNL and ECHAM) and those that use a diagnostic approach that is empirically based (GISS, MetO, LMD) or derived from a detailed aerosol/cloud droplet microphysical model (CSIRO). Other differences in the models not described in Table 2 are related to the parameterization of cloud optical depth. Most SCMs use a parameterization of the form given by *Hansen and Travis* [1974] as:

$$\tau = \frac{3 \text{ LWP}}{2 \rho_w r_e} \quad (1)$$

where ρ_w is the density of water, r_e is cloud droplet effective radii and τ is the cloud optical depth. The optical depth diagnosed in the MetO SCM for the $0.69-1.19$ μm wavelength range is from *Slingo* [1989], given as:

$$\tau = \text{LWP}\left(a + \frac{b}{r_e}\right) \quad (2)$$

where $a = 2.682 \times 10^{-2}$ (m^2 g^{-1}) and $b = 1.346$ (μm m^2 g^{-1}). In addition, the GISS SCM takes vertical subgrid scaling into account when diagnosing cloud cover and τ for

different stability conditions [*Del Genio et al.*, 1996]. The PNNL SCM scales τ in each layer by $C^{1.5}$ where C is the cloud fraction and then sums the values over all layers mimicking the random cloud overlap approach as by *Briegleb* [1992]. This produces smaller τ values and lower albedos. ECHAM takes subgrid LWC variability into account by calculating it as $CIF = 1.0 - 0.06 \text{ LWP}^{1/3}$, where CIF is the cloud heterogeneity factor [*Tompkins*, 2002], which is then used in the τ calculations.

4. Simulation Setup

[17] Below we outline four experiments set up for the SCM simulations of the June 26 and July 9 cases. When interpreting the differences between local cloud observations and model outputs, it is difficult to determine if the differences should be attributed to inappropriate meteorological conditions or to SCM parameterizations. Therefore to test model parameterizations, the following three tests were performed for a single SCM time step ($\sim$15 to 20 minutes) that commenced at 12 Z and that was initialized with the meteorological conditions locally observed with the instrumented aircraft. The objective of the fourth experiment was to test the parameterizations after the model was initialized with large-scale forcing fields so that model cloud formation and evolution could also be evaluated.

4.1. EXP-N

[18] In this experiment we test model prediction of N given either the aerosol mass or N$_a$ and cloud-scale updraft velocities (from in situ aircraft observations). The N values derived by *Pawlowska and Brenguier* [2003] were used to evaluate model predictions and examine the merits or drawbacks of the various N schemes used in the SCMs. The model was initialized with T and q$_v$ profiles from observations made during the CC campaign, except MetO and LMD, which in addition used observed LWC (this should not affect the droplet activation since they are independent of LWC).

4.2. High Vertical Resolution (HVR)

[19] *Brenguier et al.* [2003] stratified the processed microphysical data into five altitude levels regularly spaced between the observed cloud base and cloud top. The models were therefore configured with additional levels corresponding to these heights. Since these heights varied between cases, the set of model levels used for the two cases were different. Using prescribed N, cloud geometry and LWC at five different levels within the cloud, can the SCM predict the right cloud optical depth, albedo and rain? The idea behind this experiment is to test the effect of subgrid LWC variability on cloud optical depth and albedo for models that account for it and for those that do not. For precipitation, the rainwater flux predictions are compared among the SCMs to examine the effect of different autoconversion and accretion schemes currently used in the models as well as to evaluate the grid box bias when subgrid LWC variability is not accounted for.

4.3. Low Vertical Resolution (LVR)

[20] In this experiment, (b) is rerun at the standard resolution of a GCM to determine the amount of degradation that results from a coarser vertical resolution, since it is

Table 2. Model Schemes Used in the Treatment of Droplet Activation and Autoconversion (Qaut)

Processes	CSIRO	GISS	MetO	PNNL	ECHAM	LMD
Aerosol activation/droplet nucleation	Based on *Chuang and Penner* [1997] and given in terms of updraft velocity, aerosol number and anthropogenic sulfate mass. Activation parameterization is applied to a normal probability distribution of updraft velocities with the mean and standard deviation from the observed ACE-2 data set.	Empirically based as in *Menon et al.* [2002] in terms of mass of sulfates, organic, sea-salt aerosols with a dependence on cloud turbulence (uses model cloud top entrainment as a proxy for cloud turbulence).	Empirically based as in *Jones et al.* [2001] and is a function of sulfate and sea-salt aerosols.	*Abdul-Razzak and Ghan* [2001] parameterization in terms of updraft velocity, N_a, mode radius, and geometric standard deviation of lognormal size distribution. Parameters of size distribution determined by fitting observed CCN spectrum. Activation parameterization is applied to a gaussian distribution of updraft velocities.	Based on the *Leaitch et al.* [1996] scheme (function of N_a, and updraft speeds), which used a modified form of the *Ghan et al.* [1997] scheme [*Lohmann*, 2002].	Empirically based as in *Boucher and Lohmann* [1995] and is a function of sulfate mass only.
Subgrid liquid water variability	Yes	No	No	Yes	No	No
Subgrid liquid water variability for Qaut	Cloudy fraction of grid box and grid box-mean total water (liquid + freezing) calculated from the triangular probability density function of *Smith* [1990]. Cloud water in the cloudy part of the grid box is used in Qaut.	Cloudy water in the cloudy part of the grid box used in Qaut.	Same as GISS.	Triangular distribution of total water, with mean cloud water and mean auto-conversion rate determined by analytic integration	Same as GISS.	Same as GISS.

prohibitively expensive for most climate models to run at the high vertical resolution of the data analysis.

4.4. SIM

[21] In this configuration, the model was run for a 24 or 48 hr period. For models that were run for a 48 hr period, only results for the last 24 hours are shown since some models were initialized for longer durations. The simulation set-ups are briefly listed in Table 3 for each SCM since they differ from one another. Large-scale advective tendencies of T and q_v were calculated from ECMWF reanalysis. The purpose here is not so much to intercompare the SCMs but rather evaluate model cloud evolution schemes and then compare model outputs against observations. Model diagnostics of N, r_e, LWP, and cloud optical depth are averaged over the cloudy part of the grid box. This configuration mirrors a current GCM run under large-scale meteorological conditions provided by ECMWF reanalysis.

5. Simulations

5.1. Results of Single-Time-Step Diagnostic Experiments

[22] Models initialized with in situ observations are run for a single time step to evaluate droplet activation, radiation and precipitation schemes. A summary of the results is in Tables 4a and 4b, for N (EXP-N), cloud optical depth, cloud albedo and broadband albedo, as diagnosed with the SCMs successively initialized at the fine vertical resolution of the data set (HVR) and at the standard GCM vertical resolution (LVR). The MetO and ECHAM models did not participate in LVR and HVR, respectively.

5.1.1. EXP-N

[23] While the GISS, MetO and LMD SCMs require information about aerosol mass to predict N, the CSIRO, PNNL and ECHAM SCMs require additional information about cloud-scale updraft velocities and N_a as described in Table 2 and Appendix A. These models use aircraft measurements of cloud-scale updraft velocities to replace their model predicted subgrid updraft velocities (usually obtained through the turbulent kinetic energy term as indicated in Appendix A). Note that due to the single time step, the models with a prognostic scheme for droplet concentration, provide values of N right after activation, before mixing and scavenging processes are active, similarly to the models with a diagnostic scheme. For the clean case, model predicted N values are within observed ranges for all except the ECHAM and LMD SCMs. For the polluted case, only CSIRO shows values departing by more than one standard deviation from the observations. Since the N parameterization for the GISS model is empirically derived partly from measurements at Tenerife, the coincidence of observed and simulated N is not too surprising. The slight underestimation of N by MetO for the clean case is attributed to its empirical parameterization of the sea salt contribution to activated nuclei. This model does not show the same underestimation in the polluted case because of the smaller relative contribution of sea salt, against sulfate, to the total activated aerosol. Although the CSIRO model over-predicts N for both cases, the use of an alternative (diagnostic) parameterization [formula "A" of *Boucher and Lohmann*,

Table 3. Description of Simulation Setup Used in the Standard 24-hour Simulations

Setup	CSIRO	GISS	MetO	PNNL	ECHAM	LMD
Nudging	Yes	Yes.	No	No	Yes. 3-D ECHAM simulation is nudged to ECMWF and the ECHAM model is rerun for the PACE grid box, adding the missing horizontal tendencies from the 3D run to it.	Yes
Treatment of surface fluxes	Diagnosed by SCM from surface wind, temperature using Monin-Obukhov similarity theory [*Louis*, 1979].	Diagnosed by SCM from surface wind and temperature using similarity theory [*Hartke and Rind*, 1997].	Diagnosed by SCM.	Diagnosed by SCM from surface wind and temperature.	Standard GCM treatment.	Diagnosed by SCM from surface temperature and wind.
Total number of levels	18	31	30	24	19	19
Number of levels up to 720 mb	6	8	13	11	6	6
Initialization time	0z June 25 and 0z July 8	0z June 25 and 0z July 8	0z June 26 and 0z July 9	0z June 26 and 0z July 9	April 1	0z June 26 and 0z July 9

Table 4a. Results From EXP-N and Single-Time-Step Simulations for the Clean (June 26) Case for the Different SCMs and Those Retrieved From Observations (OBS)[a]

		OBS	SCM	CSIRO	GISS	MetO	PNNL	ECHAM	LMD
N (cm^{-3})	FSSP	52 ± 16	EXP-N	68	51	34	64	84	95
	OVID	46							
Cloud optical depth	FSSP	3.99 ± 2.29	HVR	3.63/7.59	3.34/8.19	3.26/6.44	3.21/7.05	NA	3.5/7
	OVID	5.09 ± 0.46	LVR	4.32/9.01	4.40/9.20	NA	5.64/12.4	3.8/7.0	3 5.5/11.4
Cloud albedo	OVID	0.19 ± 0.03	HVR	0.32/0.37	0.23/0.37	0.22/0.33	0.20/0.33	NA	0.16/0.25
			LVR	0.33/0.40	0.28/0.43	NA	0.33/0.51	0.25/0.33	0.22/0.34
Broadband TOA albedo	OVID	0.15 ± 0.01	HVR	0.26/0.30	0.19/0.30	0.18/0.27	0.17/0.27	NA	0.14/0.21
			LVR	0.27/0.32	0.23/0.35	NA	0.27/0.41	0.21/0.27	0.18/0.28

[a]For OBS both OVID retrieved and that calculated from in situ measurements (FSSP) are reported. Values from simulations run at the resolution of the data set (HVR) and from simulations run at the normal SCM resolution (LVR) are reported. Model LWP values are scaled to match both FSSP (18.5 g m^{-2}) and OVID (55.7 g m^{-2}) derived LWP values, hence resulting in two different predictions of cloud optical depth, cloud albedo and broadband TOA albedo.

1995], results in values much smaller (54 cm^{-3} and 172 cm^{-3} for the clean and polluted cases, respectively) than that from the *Chuang and Penner* [1997] parameterization. To achieve cloud droplet nucleation at the coarse vertical resolution of the ECHAM model, the measured relative humidity in the model layer corresponding to the observed cloud level had to be increased to a value (100.3%) at which nucleation occurs for the polluted case, since nucleation only occurs in a supersaturated environment. However, this artificial enhancement of the relative humidity should not have a direct impact on cloud droplet prediction since the parameterization is mainly dependent on the aerosol number, a constant c and the cloud scale updraft velocity that is obtained from aircraft measurements (equations A6 and A7) and not on the supersaturation field. We do acknowledge that this tuning of the relative humidity is indicative of the general problem faced in diagnosing boundary layer clouds and not being able to account for subgrid cloud effects on GCM grid scales. The predicted N that is obtained agrees within 2 standard deviations of the observed N for the clean case and exactly matches the observed N for the polluted case.

[24] From these results, prediction of N from aerosol mass alone may render less uncertainty, whereas, for the schemes using N_a and updraft velocity, additional variability is introduced when accounting for the updraft velocity dependence on N (that are derived from detailed aerosol microphysical models). In addition, measurements of aerosol number size distribution and sub micron aerosol chemical composition, when used to initialize detailed simulations of the activation process, generally lead to overestimation of N observed in adiabatic cloud regions. This result is seen in the work of *Hallberg et al.* [1997], and in the analysis of the ACE-2 data set [*Snider et al.*, 2003],

that reveals an over prediction by a factor of two in the worst case. Plausible explanations for the overestimation include error in the assumption that dried ambient aerosol particles are compact spheres (a common assumption), positive bias in the measurement of spectral density at accumulation mode sizes, and positive bias in field measurement of aerosol soluble mass fraction and aerosol hygroscopic properties. However, accuracy of N need not be >30% to differentiate between clean and polluted clouds and most of the models thus provide an adequate treatment of droplet activation.

5.1.2. High and Low Vertical Resolution

[25] Although in HVR all SCMs runs were at the same vertical resolution as the data set and were initialized with the observed LWC values, LWP was overestimated but within one standard deviation of in situ derived data. Therefore to facilitate the comparison of the cloud radiation parameterization between the different SCMs, LWP values were successively scaled to match those obtained from in situ and remote sensing measurements. When the SCM LWP is scaled to in situ derived values, the cloud optical depths computed are in the 3.3–4.2 range. Most of the models predict similar cloud optical depth values for both cases. The observed cloud optical depths for the clean and polluted case do not differ greatly (~6%), mostly due to the lower LWP of the polluted case as explained earlier. Scaling model LWP values to the remote sensing data tends to produce cloud optical depths that are too large for all models thus reflecting the overestimation of the remote sensing retrieved LWP.

[26] Values for cloud albedo and broadband TOA albedo are also compared with OVID estimates. Model broadband TOA planetary albedo (ratio of reflected to incoming solar radiation) is taken to be equivalent to broadband TOA

Table 4b. Similar to Table 4a but for the Polluted (9 July) Case[a]

		OBS	SCM	CSIRO	GISS	MetO	PNNL	ECHAM	LMD
N (cm^{-3})	FSSP	256 ± 38		358	217	242	216	255	241
	OVID	230							
Cloud optical depth	FSSP	4.23 ± 2.54	HVR	4.23/8.85	3.49/7.77	3.66/7.64	3.20/7.20	NA	4.00/8.50
	OVID	4.99 ± 0.45	LVR	4.93/10.4	4.73/9.90	NA	3.33/7.20	3.0/8.0	6.00/12.5
Cloud albedo	OVID	0.27 ± 0.04	HVR	0.34/0.41	0.25/0.38	0.24/0.34	0.22/0.37	NA	0.18/0.28
			LVR	0.34/0.42	0.30/0.48	NA	0.22/0.37	0.24/0.38	0.24/0.36
Broadband TOA albedo	OVID	0.18 ± 0.02	HVR	0.27/0.32	0.20/0.30	0.19/0.27	0.18/0.29	NA	0.15/0.22
			LVR	0.27/0.33	0.24/0.37	NA	0.18/0.29	0.19/0.30	0.19/0.28

[a]Model LWP values are scaled to match both FSSP (11.0 g m^{-2}) and OVID (33.4 g m^{-2}) derived LWP values, hence resulting in two different predictions of cloud optical depth, cloud albedo and broadband TOA albedo.

albedo retrieved from the remote sensing, ignoring small differences that may arise from surface contribution. For values scaled to in situ derived LWP, most SCMs come close to retrieved albedos for the polluted case, with slightly larger differences being obtained for the clean case. Despite the increase in N by more than a factor of 5 for the polluted case, none of the models show the increase in albedo, while remote sensing retrieved cloud and broadband albedos indicate a 42% and 20% increase, respectively. The reason is that the differences in cloud optical depth between the clean and polluted cases were quite small. Interestingly, the only appreciable increase in model albedo arises when LWP is scaled to the remote sensing retrieved values, i.e., when there is an increase in LWP of at least a factor of three.

[27] Since LWP variations are of importance when evaluating radiation parameterizations, it would be instructive to determine how cloud optical depth and planetary albedo are affected due to the LWP variability for models that do not explicitly account for subgrid liquid water variability (e.g., GISS, MetO, LMD). As in *Cahalan* [1994], we calculate the effective change in cloud optical depth from the observed LWP variability for the GISS SCM for the LVR case as $LWP_{eff} = \chi \overline{LWP}$, ($\chi \approx 10^{-1.15\sigma_L^2}$ is a reduction factor, σ_L is the standard deviation of $\log_{10}$LWP and LWP_{eff} is the effective LWP value). Although *Cahalan* [1994] obtained values of $\sigma_L = 0.4$ and $\chi = 0.7$ for marine stratocumulus over California, values derived for the clean and polluted case from the CC campaign are $\sigma_L = 0.33$, $\chi = 0.75$ and $\sigma_L = 0.28$, $\chi = 0.82$, respectively, with an average value of ~ 0.33 for σ_L for all 8 CC cases. The resulting decreases in the GISS model cloud optical depth for the clean and polluted case are 18% and 13% when the scaling factor is applied, with a 10% and 7% decrease in planetary albedo. A similar analysis for simulations run at the data set resolution produce reductions in planetary albedos that are 8% and 6% for the clean and polluted case, respectively. The smaller reductions that we derive may also be related to the sampling scale and cloud fraction estimates since larger areas and higher cloud fractions usually produce larger biases in albedo estimates [*Pincus et al.*, 1999; *Cahalan*, 1994]. Therefore for these two CC cases, the effect of subgrid LWP variability on planetary albedo was found to be small when using the Cahalan scaling factor as compared to differences in albedo for large changes in mean LWP. This probably also accounts for the smaller differences in albedos between models that account for subgrid LWC variability (CSIRO, PNNL and ECHAM) in cloud radiation schemes and for those that do not.

[28] The agreement between the modeled and observed cloud optical depth, cloud albedo and broadband albedo is much better when the model is applied at the vertical resolution of the observations (HVR) as compared to the results for the LVR runs. For LVR, since only one model layer may coincide with observed cloud level, LWC values at the model cloud level closest to the observed cloud level are scaled to conserve total LWP. However, now since simulated clouds are much thicker than the observed cloud (due to the coarser vertical resolution), the mean LWC for the cloud layers from observations are still not representative of the mean LWC in the simulated cloud and therefore the r_e gets smaller resulting in slightly higher cloud optical depths and albedos (especially in the GISS and LMD

models). Thus the degraded vertical resolution does not necessarily worsen the corresponding optical properties, but it is the change in LWP that causes the largest sensitivity to model radiative properties (as seen from the changes in simulated optical properties when model LWP values are scaled to OVID values). In general, cloud radiative properties are controlled by both cloud thickness and N. Hence the larger N and smaller H for the polluted case, may compensate and account for the small differences in observed radiation fluxes [*Brenguier et al.*, 2003]. The cloud thickness is determined by the meteorological conditions, while N reflects the level of pollution. Both may however be correlated since pollution involves a continental origin of the air mass, hence different meteorological conditions.

5.1.3. Choice of Autoconversion Parameterization

[29] To explore the sensitivity of model precipitation schemes, the HVR test was performed for different Qaut schemes using measured LWC profiles. A summary of model predicted rainwater fluxes for the different Qaut schemes (abbreviated as MC [*Manton and Cotton*, 1977]; TC [*Tripoli and Cotton*, 1980], BH [*Beheng*, 1994], BO [*Boucher et al.*, 1995] and KK [*Khairoutdinov and Kogan*, 2000]) is shown in Tables 5a and 5b. Model values are for cloud base, whereas, observed values are means for the entire cloud layer. Rainwater fluxes at cloud base are difficult to derive from airborne measurements because only a few aircraft legs were performed at this level during ACE-2. The best compromise for improving the statistical significance of the measurements is to calculate drizzle fluxes over all cloudy samples, from cloud base to cloud top, hence assuming the drizzle flux is uniform over the cloud depth (the procedure is described in detail in *Pawlowska and Brenguier* [2003]). This is the first source of uncertainty in the observations. The second source of uncertainty arises from the fact that most of the drizzling cases show drop volume distributions with a mode in the range between 20 and 60 μm (the two first size classes of the PMS-OAP instrument used to measure the drizzle size distribution), where the particle counting may be overestimated. Considering the instrument accuracy problem and the possible difference between cloud base and cloud mean drizzle fluxes, we note that observed fluxes could be overestimated by a factor of 5 to 10. For the non-drizzling cases, such as July 9, drizzle is sparse and there is thus larger statistical uncertainty associated with the measured precipitation rate.

[30] As seen in Table 5a for the June 26 case, some SCMs under-predict rainwater fluxes by several orders of magnitude, though MetO in the HVR simulations with either the TC or the KK schemes gets close to the observations. At the coarser resolution of the LVR simulation however, all models fail in producing noticeable precipitation rates. For the polluted case (Table 5b) all models agree in predicting negligible precipitation rates.

[31] The differences in rainwater fluxes for models using the TC scheme (GISS, MetO), or a scheme of similar form (CSIRO, LMD), can be related to the choice of critical radius used to determine the onset of auto-conversion (CSIRO = 7.5 μm, GISS = 7.5 μm, LMD = 8.0 μm) or the auto-conversion threshold (a concentration of 1000 drops per m^3 of size >20 μm is required for auto-conversion to take place in MetO). For models using the same KK scheme, (MetO, PNNL and ECHAM), given as Qaut =

Table 5a. Rainwater Fluxes (mg m^{-2} s^{-1}) From HVR for the Clean Case (June 26) for the Simulations Run at the Resolution of the Data Set (HVR) and at the Normal SCM Resolution (LVR) for the Different Autoconversion Schemes Used[a]

OBS	SCM	MC CSIRO	TC GISS	TC MetO	BO LMD	BH MetO	KK MetO	KK PNNL	KK ECHAM
25.5	HVR	0.43	0.013	3.33	0.41	6.39	0.14	0.049	NA
	LVR	0.00	0.014	NA	0.00	NA	NA	0.002	0.002

[a]MC, *Manton and Cotton* [1977]; TC, *Tripoli and Cotton* [1980]; BO, *Boucher et al.* [1995]; BH, *Beheng* [1994]; KK, *Khairoutdinov and Kogan* [2000]. Values from observations are also given.

1350 $q_c^{2.47}$ N$^{-1.79}$, (q_c is the cloud water mixing ratio) only PNNL treats subgrid variations by integrating Qaut over a triangular distribution of cloud water mixing ratio. Thus despite similar LWC profiles and N, the use of a subgrid variability scheme and different thresholds may produce differing ranges of rainwater fluxes for models that use similar Qaut schemes. Another reason for the differences could be related to the different accretion schemes used in the models, described in Appendix A, which may cause more rapid collection in some models as opposed to the others. None of the models considered subgrid variability in accretion, assuming that cloud water and rainwater are uncorrelated, which may not be justified and may explain the underestimation of rainwater fluxes.

[32] Since most precipitation schemes are from cloud resolving models, the coarser GCM grid cells typically introduce some biases when subgrid LWC variability is not accounted for [*Pincus and Klein*, 2000]. The bias rates can be computed as by *Wood et al.* [2002] for three approaches using: (a) a homogenous LWC; (b) the grid box mean LWC and cloud fraction but assuming cloud internal homogeneity; and (c) a Gaussian framework to treat subgrid LWC variability by assuming that the saturation excess follows a Gaussian distribution. These three scenarios are described as the homogeneous, black-white and Gaussian models. For MetO, scenario (a) is implemented, using the grid-box mean LWC to calculate grid-box mean auto-conversion rate, which is then corrected using the form of *Wood et al.*'s equation (30) that is expressed in terms of the grid-box mean LWC. For GISS, scenarios (b) and (c) are implemented, using *Wood et al.*'s equations (6) and (21) respectively. The correction factors applied to remove the Qaut bias for each scenario are given as:

$$GACB_{Hom} = \exp\left(\frac{-\bar{q}_c}{G(L)}\right) \quad (3)$$

$$GACB_{BW} = 1 - \frac{(\overline{q_c})^\alpha}{C^{\alpha-1}\overline{q_c^\alpha}} \quad (4)$$

$$GACB_{Gauss} = 1 - \frac{\sigma_s^\alpha I(\alpha, -Q_1)}{\sqrt{2\pi}\,\overline{q_c^\alpha}} \quad (5)$$

where $GACB_{Hom}$, $GACB_{BW}$ and $GACB_{Gauss}$ are the grid-box Qaut biases for (a), (b) and (c), respectively. *C* is the cloud fraction, α is the exponent of q_c used in the Qaut equation (e.g., 2.47 for the KK scheme), σ_s is the standard deviation of the function s, where s depends on the grid box total water content, the liquid water potential temperature and the saturation specific humidity and $I(\alpha, -Q_1)$ is the αth Gaussian partial moment integral given in an analytical form in terms of the $1F1$-hyper geometric function. Q_1 is the normalized saturation excess given as a function of the grid-box total water content, the saturation specific humidity, σ_s, temperature, and the specific heat of vaporization of water. $G(L)$ a function of the run length, L (horizontal scale in km), is defined as $1.15(\alpha - 1)\sigma_s$. The correction factor to be applied to the Qaut rate is:

$$F = \frac{1}{1 - GACB} \quad (6)$$

[33] In MetO, biases are calculated for different Qaut schemes with the BH scheme exhibiting the largest bias followed by the KK scheme, reflecting the relative sizes of α in the 3 schemes. The application of GACB correction factors produce rainwater fluxes that are closer to observed ones, as shown in Tables 6a and 6b. Since the second indirect effect is highly sensitive to the precipitation scheme, accounting for subgrid LWC variability is more likely to improve predictions of rainwater fluxes. Here, we only discuss the onset of precipitation vis a vis the Qaut scheme though the production of precipitation is also determined by the accretion scheme whose contribution to total precipitation is estimated to be an order of magnitude larger than Qaut for the ACE-2 cases [*Pawlowska and Brenguier*, 2003]. However, a systematic intercomparison of Qaut and accretion rates is not available for all models, (Qaut is higher than accretion in the GISS SCM whereas PNNL indicates higher accretion rates). We mainly focus on Qaut rates, since it is the trigger for the precipitation while aerosols affect the accretion process indirectly via Qaut.

5.2. Results of 24-hour Simulations From SIM

5.2.1. Cloud Morphology

[34] To evaluate the SCM's ability to form clouds, we compare the 24 hour cloud evolution with that from ISCCP data and in situ observations when available. Model simulated cloud fractions are shown in Figures 1a and 1b for June 26 and July 9, respectively. In situ observed values of cloud base and top (at 12Z) are superimposed on the upper-

Table 5b. Similar to Table 5a but for the Polluted Case (9 July)

OBS	SCM	MC CSIRO	TC GISS	TC MetO	BO LMD	BH MetO	KK MetO	KK PNNL	KK ECHAM
2.22	HVR	0.00	0.00	0.83	0.00	0.005	0.003	0.009	NA
	LVR	0.00	0.07	NA	0.00	NA	NA	0.009	1.0e-4

Table 6a. Similar to Table 5a but With the Bias Rates Accounted for in the GISS and MetO SCMs for Three Different Scenarios as by *Wood et al.* [2002] for Different Autoconversion Schemes[a]

OBS	Scenarios	TC GISS	TC MetO	BH MetO	KK MetO
25.5	Uncorrected	0.013	3.33	6.39	0.14
	Homogeneous		7.22	16.7	0.33
	Black-White	0.13			
	Gaussian	0.79			

[a]Note that values are only given for the simulations run at the data set resolution (HVR). For convenience, uncorrected rainwater fluxes from Table 5a are also given.

left graph (CSIRO) (cloud thickness is ∼202 and 167 m for the clean and polluted case, respectively). These are compared to ISCCP 3 hourly cloud fractions and cloud tops, (at the ECMWF reanalysis resolution) shown in Figure 2 that are similar to cloud fractions from casi: 0.78 and 0.75 for June 26 and July 9. Radiosonde measurements at 32.6N and 16.9W, along with aircraft soundings and the simulated profiles are reported at 12 Z in Figure 3. Prominent features in cloud fields are the change in the cloud base placement for the clean vs. polluted case and the thinner cloud for the polluted case captured by most models though simulated cloud bases are much lower. Also, the observed higher cloud water mixing ratios (g/kg), q_c, of the clean air mass compared to that of the polluted one are not reflected by the models (Figures 4a and 4b) since the ECMWF soundings used to initialize the models have slightly higher moisture contents for July 9, in contrast to in situ observations (and back trajectory analysis). Thus noticable differences between aircraft and ECMWF soundings present an obstacle in the comparison of local observations with model outputs. Besides problems with ECMWF soundings, sampling issues (60 km CC domain versus the 250 km ISCCP and ECMWF resolution) may cause additional complications. Data from the spaceborne multidirectional radiometer (POLDER) at a 6.2 km resolution available for June 26, indicate low-level broken clouds with high spatial variability [*Parol et al.*, 2000]. Analysis of ISCCP products at $0.5° \times 0.5°$ resolution did not narrow this discrepancy that may imply the presence of thin clouds, which are more difficult to verify.

[35] Thus several discrepancies exist in the comparison of simulated and observed cloud fields that are difficult to disentangle mainly due to the inadequacy of the reanalysis forcing used for initializing boundary layer cloud simulations. Understanding aerosol impacts on cloud evolution will not occur unless soundings at multiple locations are also available to characterize advective forcings. Of relevance is the overestimation of cloud thickness by all models except the GISS and MetO SCMs that may be easier to resolve. The subgrid cloud thickness scheme in the GISS SCM, described in *Del Genio et al.* [1996], makes the cloud physically thinner than the SCM layer thickness by distributing the cloud evenly in all 3 dimensions for stable situations. Despite a coarse vertical resolution in the lower boundary layer, the scheme may eliminate excessively thick clouds, which then result in lower LWP and cloud optical depth estimates. The MetO SCM, the only model with cloud base at slightly higher levels, has the finest boundary layer resolution, as seen in

Table 3 that may enable it to better resolve surface and boundary layer variables used to diagnose clouds. Further, the use of the *Lock* [2001] boundary layer scheme allows the MetO SCM to resolve subgrid inversions, enabling more accurate diagnosis of boundary layer clouds. Although we do not rule out the possibility that improved large-scale forcing may have improved model cloud morphology predictions, we believe that subgrid schemes may be more realistic since most cloud processes have non linear process rates that have to be represented adequately.

5.2.2. Cloud Microphysical Properties

[36] The noticable difference between the large-scale ECMWF reanalysis fields and the vertical T and q_v profiles measured locally results in simulated cloud layers that are thicker than the observed ones. As a result, model predicted values of LWP, optical depth, cloud albedo and broadband albedo are significantly overestimated, with respect to the observed ones (not shown). Considering the overestimation of the predicted LWP, it might be anticipated that the precipitation rate would also be overestimated, while all models predictions are in fact underestimated with respect to observations (due to the problems listed in Section 5.1.3).

[37] SIM also highlights the numerical sensitivity of the prognostic parameterization of N. This feature is illustrated by the polluted case predictions of PNNL and ECHAM, both using a prognostic scheme, as opposed to models using a diagnostic scheme. Diagnostic predictions of N are close to the observed one (overestimated by CSIRO and GISS for July 9) as shown in Figure 5 (top). The LMD model over-predicts N by 50% for June 26 (the simulated sulfate mass from the on-line sulfate chemistry model exceeds the measured value by ∼28%); while the predicted N agrees with observed N for July 9 (predicted sulfate mass is ∼22% lower than the observed value) at 12Z. Using the observed aerosol mass results in values of N that are quite similar to the simulated sulfur cases for June 26 and July 9 at 12Z. This suggests that the equation used to predict N from sulfate (equation A8) is not too sensitive to small changes (∼<30%) in sulfate concentration, but may be more sensitive to low sulfate values and may overestimate sulfate contribution to N.

[38] With the two prognostic schemes (Figure 5, bottom) however, the results are more contrasted, because of a feedback loop between N and precipitation: N (together with LWP) determines the droplet size that is compared to the auto-conversion threshold for the onset of precipitation. The initial diagnostic of aerosol activation in PNNL (source term) results in a large N value (the simulated turbulent updraft velocity required by its parameterization is much stronger than the observed one: the variance of simulated updraft velocity is about 2 m^2 s^{-2} on both June 26 and

Table 6b. Same as Table 6a but for the Polluted Case (9 July)

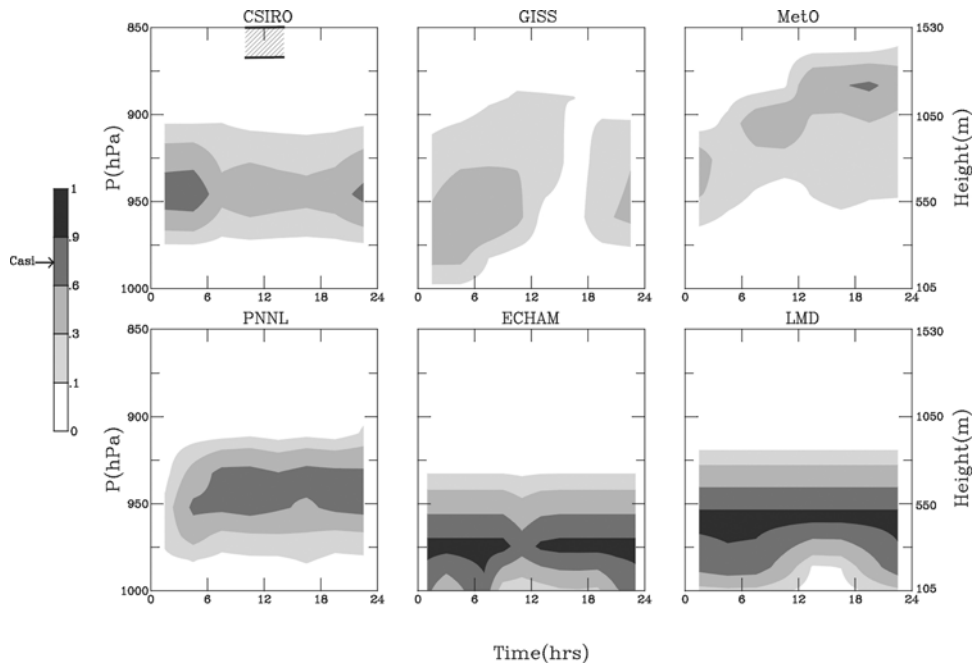| OBS	Scenarios	TC GISS	TC MetO	BH MetO	KK MetO
2.22	Uncorrected	0.00	0.83	0.005	0.003
	Homogeneous		2.22	0.023	0.011
	Black-White	0.00			
	Gaussian	0.00			

Figure 1a. Time-pressure plot of the predicted cloud fraction for the clean case (26 June). Observed cloud base and top levels are reported in the upper left graph (CSIRO). Cloud fraction from observations (casi) are also indicated on the color bar.

July 9, while the observed variance was 0.15 on June 26 and 0.25 on July 9), thus preventing the formation of precipitation, so that the prognostic value remains close to the initial value. In contrast, ECHAM nucleates a lower N, hence allowing the formation of precipitation. Drizzle then scavenges the droplets (sink term), thus reinforcing the formation of precipitation by auto-conversion, until N is almost completely depleted (Figure 6). Values of N simulated with and without the prognostic scheme indicate that

the source/sink terms for N may deplete the population much faster than observed.

6. Discussion and Conclusions

[39] Single column versions of six GCMs have been tested against selected case studies of the ACE-2 Cloudy Column field experiment to evaluate their ability at reproducing the observed cloud layers, their radiative properties,
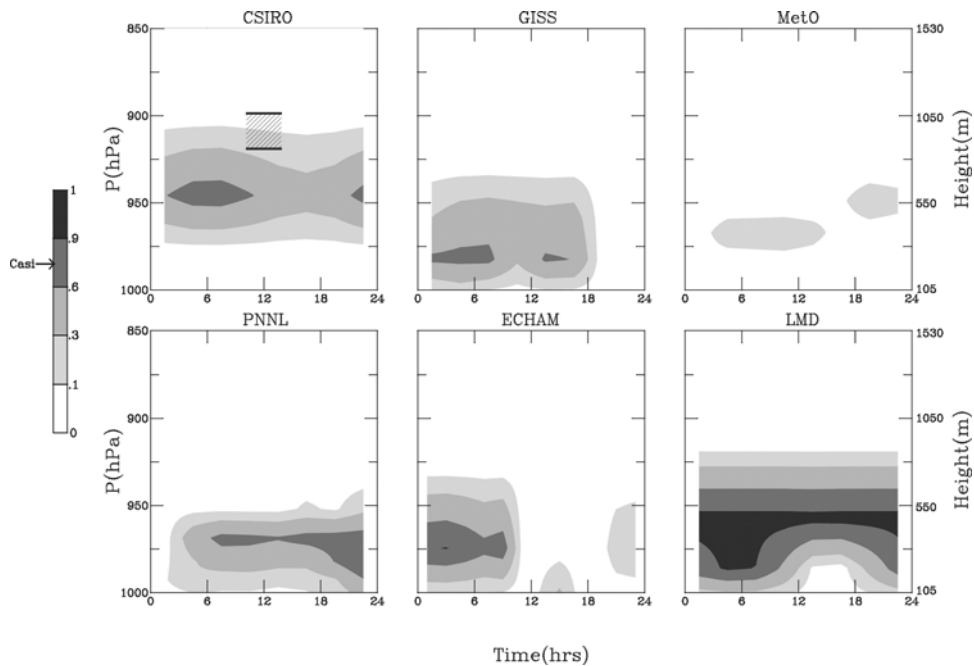
Figure 1b. Similar to Figure 1a but for the polluted case (9 July).
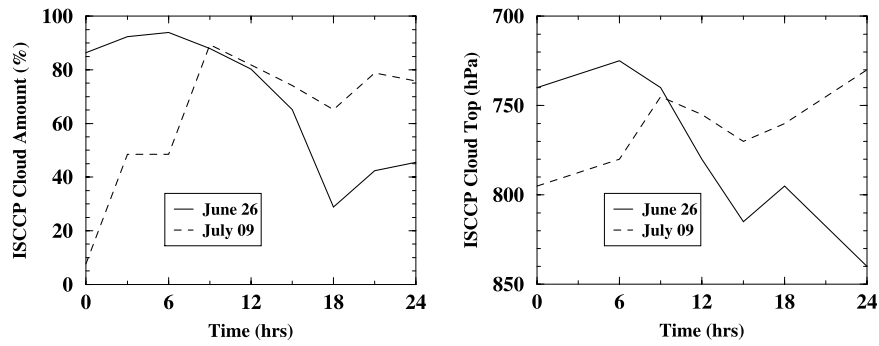
Figure 2. Time series of ISCCP retrieved cloud amount and cloud top levels for the clean (26 June) and the polluted case (9 July).

and more specifically for identifying limitations of aerosol/cloud/radiation interactions within the range of uncertainty in in situ, reanalysis and satellite retrieved data. The SCMs have been initialized with measured aircraft soundings from the CC domain and with large-scale forcing fields from the ECMWF reanalysis over the ACE-2 period (June–July 1997). SCM runs have been performed for two selected cases: June 26 (clean case) and July 9 (polluted case), (a) for single time steps (to evaluate model activation, radiation and precipitation schemes) and (b) for a 24/48 hour period (to evaluate, in addition, cloud formation and evolution). The single time step runs have been performed first with the same vertical resolution as observations and second with the current vertical resolution of the parent GCMs, to discriminate between inaccuracy of the parameterizations and the degradation of the prediction that only arises from the coarse GCM vertical resolution.

[40] The main conclusions from these exercises are: (1) Results from the droplet activation experiments suggest that the physically based schemes, though more fundamental, do not outperform the simpler empirically based schemes because they are controlled by vertical velocities at scales not resolved by GCMs; and the coupling between droplet source and loss terms cause additional discrepancies in prognostic schemes compared to the diagnostic ones. (2) Most of the GCM parameterizations under-predict precipitation formation in marine stratus but do somewhat better when subgrid LWC variability is accounted for. (3) ECMWF reanalysis products are inadequate to force SCMs for marine stratocumulus cloud simulations and this deficiency is pronounced when investigating aerosol effects since dynamics affects these clouds as much as aerosols do. (4) Subgrid cloud thickness and inversion parameterizations help improve cloud macrostructure.
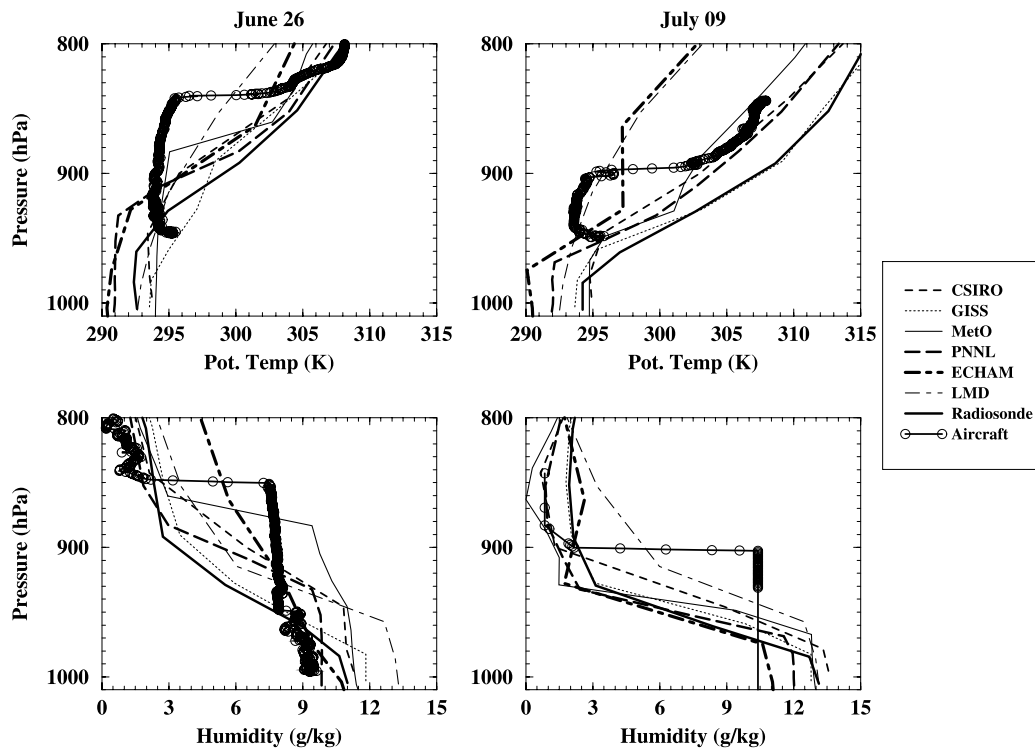

Figure 3. Potential temperature (T) and humidity (q_v) soundings from the 6 SCMs, aircraft data, and radiosonde for the clean and polluted case at 12Z.
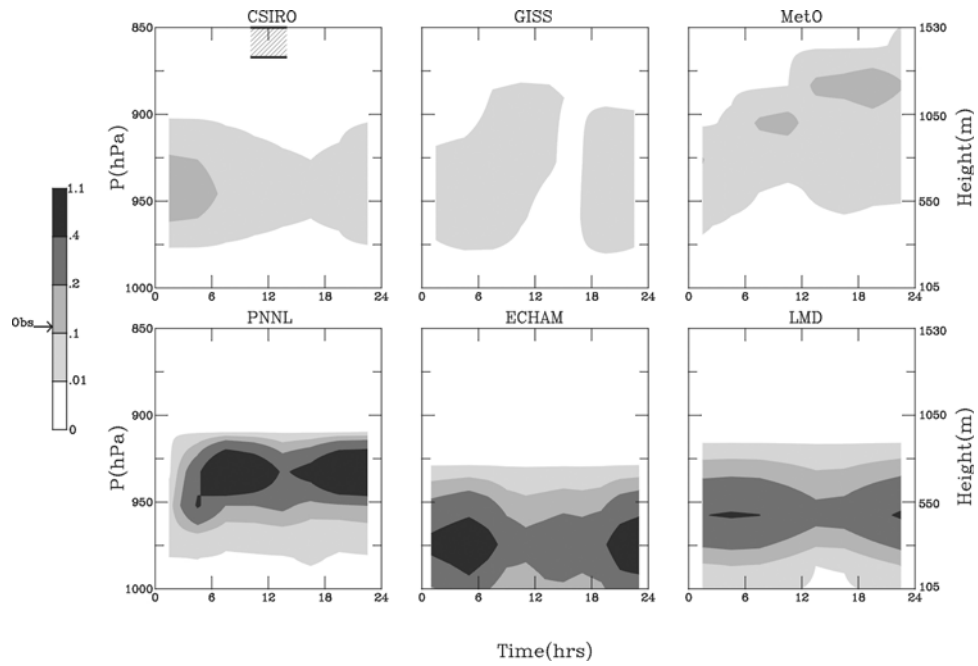
Figure 4a. Similar to Figure 1a but for cloud water mixing ratio (g/kg). Observed values are also indicated on the color bar.

[41] Comparing results from the single time step and the 24/48 hour simulations indicate that prescribing cloud LWC and geometry, as was done in the single time step runs, removes the largest source of error in model simulations - that of simulating the cloud morphology. Consequently, quantities that depend on cloud LWC and geometry, such as cloud optical depth and albedo, were much better predicted when the vertical LWC profile was prescribed. Although the albedo of polluted clouds are generally higher than that of clean clouds, based on the two cases simulated in this study, the cloud optical depth or albedo is not a good indicator of the degree of pollution (more evident by changes in N) due to the LWP differences between the clean and polluted cases, which suggests that meteorological conditions associated with air masses may affect clouds in a way that offsets or exaggerates the indirect aerosol effect.

[42] The problems associated with the aerosol indirect effect are linked to broader issues related to large and small-
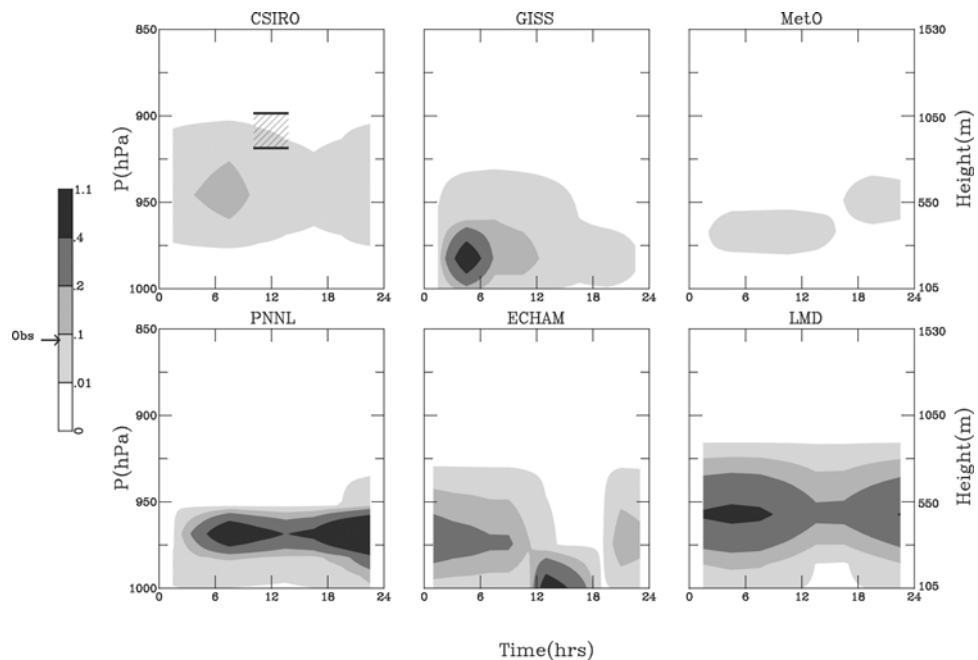
Figure 4b. Similar to Figure 4a but for the polluted case (9 July).
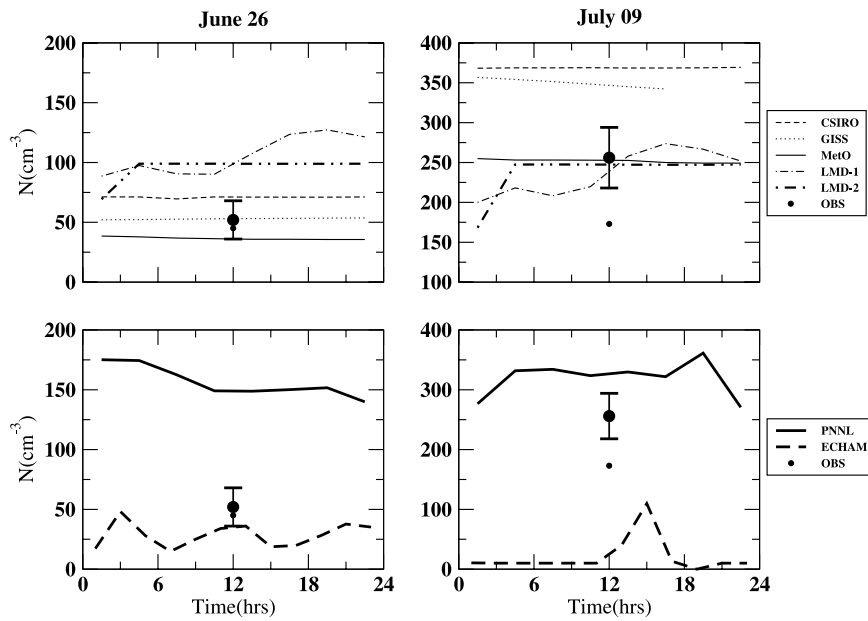
Figure 5. Time series of predicted cloud droplet number concentration (N) for the clean and polluted cases for the diagnostic (upper panels) and prognostic (lower panels) schemes. Observations, plotted at 12 Z, are from in situ measurements averaged from 12 Z to 15 Z. For observed N, two values are indicated: N for selective sampling and representative of aerosol impacts on clouds as described in Section 2.1 and the average N for all conditions (including mixing and scavenging) that have lower values of 45 cm^{-3} and 173 cm^{-3} for June 26 and July 9, respectively. Two values for LMD are N predicted from simulated aerosol mass (LMD-1) and N predicted from observed aerosol mass (LMD-2).

scale dynamical problems and cannot be evaluated in isolation of the more general problems associated with the parameterization of clouds. The collaboration between experimentalists and modelers in this study provided an useful opportunity to evaluate the importance of variables used in the parameterizations of the aerosol indirect effect listed in decreasing order of importance as (a) large-scale vertical velocity fields, (b) cloud droplet number (from activation), cloud thickness or LWP; (c) the probability distribution function of LWC, and (d) that of the updraft velocity needed for activation and its relation to the subgrid turbulent kinetic energy. To date, there are no known approaches or measurements that provide an accurate determination of cloud thickness or LWP (over land) on a global scale. As suggested by *Brenguier et al.* [2003], it is the relationship between N and cloud thickness that may prove to be more useful in diagnosing the relationship between cloud optical depths and r$_e$ that are usually used to monitor the magnitude and sign of the first indirect effect. Thus future studies that characterize the variability in cloud thickness and LWP, i.e., of dynamics, should be encouraged so that the first indirect effect can be constrained and accurately parameterized. In the context of the second indirect effect, observations of light drizzle rates need to be improved. Airborne measurements with particle counters are inaccurate when particles are small and sparse, but significant improvements could be obtained from airborne radars that sample large cloud volumes [*Stevens et al.,* 2003]. Large-scale model parameterizations of the autoconversion and accretion schemes clearly need further work, especially the scaling arguments needed for commu-
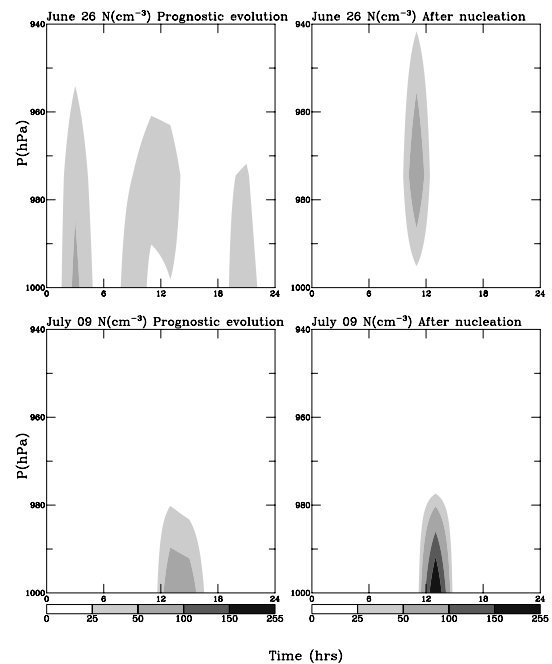

Figure 6. Time-pressure plot of the ECHAM simulation of cloud droplet number concentration (N) that shows the differences in N when N is treated prognostically and when N is calculated right after nucleation for the clean (26 June) and the polluted case (9 July).

nicating results obtained from cloud resolving model scale to the GCM scale.

Appendix A: Brief Description of Relevant Features of the Six SCMs Used in This Study

A1.   CSIRO

[43] The CSIRO SCM is a single column version of the CSIRO climate model, which has 18 hybrid sigma-pressure vertical coordinate levels with a model top at 0 hPa. The treatment of stratiform clouds and precipitation is described as by *Rotstayn* [1997]. The scheme includes prognostic variables for cloud-liquid water and cloud ice, a fractional cloudiness scheme, and physically based treatments of the microphysical conversion terms. An improved treatment of mixed-phase clouds [*Rotstayn et al.*, 2000] is also included in the SCM. The cloud water auto-conversion scheme is based on *Manton and Cotton* [1977], and the accretion scheme for the collection of cloud liquid water by raindrops generated in the grid box by auto-conversion and by those that fall into the grid box from the layer above is based on the integration of the continuous-collection equation over the Marshall-Palmer distribution that also accounts for the fall speed of raindrops and is given by *Rotstayn* [1997]. Although the CSIRO model treats subgrid LWC variability [*Rotstayn*, 2000], it is not included in the SCM auto-conversion scheme in this study mainly because the change in simulated water vapor mixing ratios w.r.t observations is quite large when subgrid LWC variability is introduced. This is true when nudging is not included in the simulations. When nudging is included, difference between simulations with and without subgrid LWC variability is small. Therefore to minimize differences between the nudged vs. non-nudged simulations of the water vapor mixing ratio, subgrid LWC variability is not treated for auto-conversion. The model has a mass-flux based convection scheme [*Gregory and Rowntree*, 1990], which also includes a treatment of shallow convection.

[44] Aerosol/cloud droplet number parameterization is based on *Chuang and Penner* [1997], in which cloud droplet number is parameterized in terms of local aerosol number, anthropogenic sulfate mass concentration, and updraft velocity.

$$N = \frac{wN_a}{w + cN_a}, \quad (A1)$$

where N_a (cm^{-3}) is the total aerosol number concentration and ω is the updraft velocity in cm s^{-1}, the coefficient c is expressed as $c = 0.04095 + 21.587\, X_L$ over land and $c = 0.02215 - 0.1329\, X_O + 3.0737\, X_O^2$ over ocean.

$$X_L = (\log w)\big[1 - (\log w)\big(0.5 + \gamma/\alpha^4\big) \\ /(\log N_a)^2\big]/(\log N_a)^{5+\gamma/\alpha^3} \quad (A2)$$

$$X_O = (\log w)\Big[1 - (\log w)\big(0.5 + 0.2\gamma/\alpha^3\big)/(\log N_a)^2\Big] \\ /(\log N_a)^{2+0.1\gamma/\alpha^2} \quad (A3)$$

where α is referred to as the shape parameter for the anthropogenic sulfate-containing aerosol distribution and is

defined as the ratio of anthropogenic sulfate loading (in µg m^{-3}) to the total aerosol number (in 1000 cm^{-3}). γ is the ratio of the fraction of anthropogenic sulfate converted by the aqueous pathway to the mean values (=75%). The long-wave radiation parameterization follows *Schwarzkopf and Fels* [1991] and the short-wave radiation parameterization uses an improved version of *Lacis and Hansen* [1974].

A2.   GISS

[45] The GISS SCM adapted from the GISS Model II' GCM [*Hansen et al.*, 1997], is a grid point model with 31 vertical sigma coordinate levels and a dynamical top at 10 hPa. The SCM has a prognostic cloud water scheme for stratiform clouds [*Del Genio et al.*, 1996] and a stratiform cloud cover scheme that is relative humidity dependent, based on the approach of *Sundqvist et al.* [1989], but also includes a dependence on moist stability. The cumulus parameterization is based on mass flux closure [*Del Genio and Yao*, 1993] and has been evaluated with observations from the Atmospheric Radiation Measurement (ARM) observations [*Xie et al.*, 2002]. Fractional cloudiness occurs in the vertical as well as horizontal, i.e., a cloud physical thickness that is less than the SCM layer thickness, depending on stability. Microphysical sinks for liquid water include auto-conversion, evaporation, cloud-top entrainment, accretion, and the Bergeron-Findeisen process. Model rain rate is determined using the auto-conversion parameterization of *Tripoli and Cotton* [1980] and an efficiency factor that accounts for the accretion of cloud water by precipitation [*Del Genio et al.*, 1996].

[46] The parameterizations used to evaluate the AIE are similar to those described by *Menon et al.* [2002] except that the chemistry model is decoupled in the SCM. N is diagnosed from the measured sulfate, organic matter and sea-salt mass through an empirical relationship given as:

$$N = 10^{[2.41+0.5\,\log(\text{Sulfate})+0.13\,\log(\text{OM})+0.05\,\log(\text{Sea-salt})]} \quad (A4)$$

where sulfate, OM and sea-salt are the mass concentrations in µg m^{-3} and N is in cm^{-3} [*Menon et al.*, 2002]. The GCM's parameterization of cloud top entrainment (CTE) is used as an indicator of within-cloud turbulence and N is scaled by a factor that ranges from 1.5 in high CTE (unstable, strong turbulence) conditions to 0.5 in zero CTE (extremely stable, weak turbulence) conditions. The radiation scheme includes all the important radiatively active species; it uses the correlated k-distribution approach for gaseous absorption and a single Gauss point adaptation of the doubling and adding method for multiple scattering.

A3.   MetO

[47] The Hadley Centre experiments were based on a single column version of the HadAM4 configuration of the Met. Office's Unified Forecast/Climate model. This in turn was developed from the earlier HadAM3 configuration described by *Pope et al.* [2000]. The cloud scheme is based on that of *Smith* [1990]. The radiation scheme is that of *Edwards and Slingo* [1996], with 6 bands in the solar region of the spectrum and 9 in the thermal infrared region. Cloud overlaps are treated using the maximum/random approach, whereby clouds in adjacent model layers are assumed to

overlap maximally but disjoint layers of cloud overlap randomly.

[48] The treatment of aerosol-cloud interaction is exactly as described by *Jones et al.* [2001], though in the present experiments the aerosol quantities were prescribed rather than being simulated interactively. Measurements of aerosol composition made at PDH were used to specify the mass mixing ratio of non-sea-salt sulfate and the number concentration of sea-salt particles. The same size distribution assumption used in the GCM was used to convert the sulfate values to number concentrations. The parameterization is given as:

$$N = 3.75 \times 10^8 \left[1 - \exp(-2.5 \times 10^{-9}\,N_a) \right] \qquad \text{(A5)}$$

where N is droplet concentration and N_a is total aerosol number (sea-salt plus sulfate). N is held to a minimum value of 5.0×10^6 m^{-3} over the ocean. The parameterization of drizzle production by auto-conversion is again handled in the same way as explained by *Jones et al.* [2001], using the scheme due to *Tripoli and Cotton* [1980], except where noted otherwise. Accretion is parameterized as a simple collision-collection process, where raindrops are assumed to follow an exponential (Marshall-Palmer) size distribution, and collection efficiency is unity. The one aspect in which the physics of the model used in this work differs from HadAM4 is in the choice of boundary layer scheme. Here, we use the parameterization developed by *Lock* [2001].

A4. PNNL

[49] The Pacific Northwest National Laboratory (PNNL) SCM is a single column version of the PNNL version of the National Center for Atmospheric Research (NCAR) community climate model (CCM2). Droplet number is determined by integrating the droplet number balance [*Ghan et al.*, 1997] in time, with separate treatments of nucleation, vertical mixing, and droplet loss due to evaporation, auto-conversion, and collection by rain. Droplet nucleation is parameterized in terms of updraft velocity, aerosol hygroscopic properties, and the parameters of a lognormal aerosol size distribution [*Abdul-Razzak and Ghan*, 2000], integrating over an assumed gaussian subgrid frequency distribution of updraft velocity, with the vertical velocity variance related to the turbulence kinetic energy. The scheme also includes the dependence of droplet nucleation on the subgrid distribution of cloud cover and cloud overlap. The triangular subgrid frequency distribution of total water [*Smith*, 1990] is used to analytically diagnose the grid cell mean cloud fraction, cloud liquid water content, and auto-conversion rate. The variance of total water is determined from a turbulence closure scheme. The *Khairoutdinov and Kogan* [2000] auto-conversion parameterization is used, assuming auto-conversion does not affect the mean droplet size. Collection by rain is parameterized as the product of the cloud water mixing ratio, rain mixing ratio, and a size-dependent droplet collection efficiency [*Tripoli and Cotton*, 1980].

[50] The in-cloud cloud optical depth, single-scattering albedo, and asymmetry parameter for cloud water are parameterized by *Slingo* [1989]. The droplet effective radius is expressed in terms of the in-cloud water mass mixing ratio and droplet number mixing ratio according to *Martin et al.* [1994]. Cloud overlap is treated by scaling the in-cloud cloud optical depth by $C^{1.5}$.

A5. ECHAM

[51] The ECHAM experiments were based on a single column version of a preliminary version of the ECHAM5 climate model, which was developed from the earlier ECHAM4 configuration described by *Roeckner et al.* [1996]. The cloud scheme predicts the number concentrations of cloud droplets and ice crystals and the mass mixing ratios of cloud water and cloud ice [*Lohmann et al.*, 1999 and *Lohmann*, 2002] and includes the prognostic cloud cover scheme developed by *Tompkins* [2002]. The radiation scheme is that of *Gregory et al.* [2000] and *Mlawer et al.* [1997]. Cloud overlaps are treated in a similar way as in the MetO SCM.

[52] The treatment of aerosol-cloud interaction is described by *Lohmann et al.* [1999], though in the present experiments N_a is prescribed from measurements of aerosol composition at PDH, rather than being simulated interactively. Cloud droplet activation (Q_{nucl}) is parameterized according to *Lin and Leaitch* [1997] based on observational data from the North Atlantic Regional Experiment:

$$Q_{nucl} = \max\left\{ \frac{1}{\Delta t} \left(0.1\,N_{max}^{1.27} - N_{old} \right), 0 \right\} \qquad \text{(A6)}$$

$$\text{where,} \quad N_{max} = \frac{N_a \omega}{\omega + c N_a}, \qquad \text{(A7)}$$

and c = 0.023 cm^4 s^{-1} and ω is the updraft velocity given as $\omega = \varpi + 1.33\sqrt{\text{TKE}}$, where ϖ is the mean vertical velocity in grid box and TKE is the turbulent kinetic energy. The parameterization of drizzle production by auto-conversion is done using the scheme of *Khairoutdinov and Kogan* [2000] and that for accretion is given as a function of the product of cloud water and rainwater mixing ratios as in *Khairoutdinov and Kogan* [2000]. The ECHAM approach to nudge the SCM deviates from the other simulations. A three-dimensional simulation is nudged toward ECMWF analyses that started on April 1, 1997. The advection of temperature and moisture into the column as well as surface fluxes, temperature and pressure over the ACE2 period were saved and used in the subsequent SCM simulations as boundary conditions.

A6. LMD

[53] The experiments described are based on a single-column version of the Laboratoire de Météorologie Dynamique (LMD) GCM. The condensation scheme applies a "hat" probability density function of total water mixing ratio as described by *Le Treut and Li* [1991]. N is derived from sulfate aerosol mass concentration using the empirical formula of *Boucher and Lohmann* [1995, their formula "D"] and is given as:

$$N = 10^{\left[2.21 + 0.41 \times \log\left(SO_4^{-2} \right) \right]} \qquad \text{(A8)}$$

where N is the droplet number concentration in cm^{-3} and SO_4^{-2} is the sulfate mass in μg m^{-3}. A scheme treating the warm microphysical processes is applied in the model

following *Boucher et al.* [1995]. The auto-conversion rate is related to $q_c^{7/3} N^{1/3}$. The accretion term is based on the integration of the continuous-collection equation over the Marshall-Palmer distribution and also accounts for the fall speed of raindrops that is related to the square root of the droplet radius as in *Tripoli and Cotton* [1980]. A random overlap assumption is used for the cloud fraction. The solar radiation parameterization is an updated version of *Fouquart and Bonnel* [1980] and the long-wave radiation scheme is based on *Morcrette* [1991].

[54] The LMD SCM uses a different setup for the 24 hr simulations. To initialise and force the model, a 3D GCM run is nudged to ECMWF data and zoomed over the region of interest, with the center of the zoom at 16.5°W and 29.5°N. The model is vertically discretized on 19 hybrid sigma-pressure levels with a 30 minutes time step. In the zoom area, a grid mesh has a horizontal resolution of 139 km by 91 km. An on-line sulfur cycle is used to calculate sulfate aerosols [*Boucher and Pham*, 2002; *Boucher et al.*, 2002]. The model was initialised using ECMWF data with a spin-up from January 1st 1997 to obtain sulfate concentrations at equilibrium. Daily-mean SSTs are imposed, using the Reynolds SST dataset [*Reynolds and Smith*, 1995]. The temperature and the horizontal wind were nudged to ECMWF data using a relaxation time constant of 0.1 day and 1 day for the wind and the temperature, respectively. Model values at the point (17.4°W/29.5°N) are used to initialise the SCM. 3-D GCM values of temperature, wind, humidity, and surface pressure are taken to force the SCM. While the winds and the surface pressure are imposed on the model, temperature and humidity are relaxed using the relaxation constant from *Ghan et al.* [1999] as described in Section 2.2.

References

Abdul-Razzak, H., and S. J. Ghan, A parameterization of aerosol activation. 2: Multiple aerosol types, *J. Geophys. Res.*, *105*, 6837–6844, 2000.
Albrecht, B. A., Aerosols, cloud microphysics, and fractional cloudiness, *Science*, *245*, 1227–1230, 1989.
Albrecht, B. A., C. S. Bretherton, D. Johnson, W. H. Scubert, and A. S. Frisch, The Atlantic stratocumulus transition experiment - ASTEX, *Bull. Am. Meteorol. Soc.*, *76*, 889–904, 1995.
Beheng, K., A parameterization of warm cloud microphysical conversion processes, *Atmos. Res.*, *33*, 193–206, 1994.
Boucher, O., and U. Lohmann, The sulfate-CCN-cloud albedo effect. A sensitivity study with two general circulation models, *Tellus*, *47B*, 281–300, 1995.
Boucher, O., and M. Pham, History of sulfate aerosol radiative forcings, *Geophys. Res. Lett.*, *29*(9), 1308, doi:10.1029/2001GL014048, 2002.
Boucher, O., H. Le Treut, and M. B. Baker, Precipitation and radiation modeling in a general circulation model: Introduction of cloud microphysical processes, *J. Geophys. Res.*, *100*, 16,395–16,414, 1995.
Boucher, O., M. Pham, and C. Venkataraman, Simulation of the atmospheric sulfur cycle in the Laboratoire de Météorologie Dynamique General Circulation Model. Model description, model evaluation, and global and European budgets, *Sci. Note of the IPSL*, ISPL, Simon Laplace, France, 2002.
Brenguier, J.-L., H. Pawlowska, L. Schüller, R. Preusker, J. Fischer, and Y. Fouquart, Radiative properties of boundary layer clouds: Droplet effective radius versus number concentration, *J. Atmos. Sci.*, *57*, 803–821, 2000a.
Brenguier, J.-L., P. Y. Chuang, Y. Fouquart, D. W. Johnson, F. Parol, H. Pawlowska, J. Pelon, L. Schüller, F. Schröder, and J. R. Snider, An overview of the ACE-2 CLOUDYCOLUMN closure experiment, *Tellus*, *52B*, 814–826, 2000b.
Brenguier, J.-L., H. Pawlowska, and L. Schüller, Cloud Microphysical and radiative properties for parameterization and satellite monitoring of the indirect effect of aerosol on climate, *J. Geophys. Res.*, in press, 2003.
Briegleb, B. P., Delta-Eddington approximimation for solar radiation in the NCAR Community Climate Model, *J. Geophys. Res.*, *97*, 7603–7612, 1992.
Cahalan, R. F., Bounded cascade clouds: Albedo and effective thickness, *Nonlin. Proc. Geophys.*, *1*, 156–167, 1994.
Chuang, C., and J. E. Penner, An assessment of the radiative effects of anthropogenic sulfate, *J. Geophys. Res.*, *102*, 3761–3778, 1997.
Del Genio, A. D., and M.-S. Yao, Efficient cumulus parameterization for long-term climate studies: The GISS scheme, *Am. Meteorol. Soc.*, *46*, 181–184, 1993.
Del Genio, A. D., M.-S. Yao, and K. K.-W. Lo, A prognostic cloud water parameterization for global climate models, *J. Climate*, *9*, 270–304, 1996.
Edwards, J. M., and A. Slingo, Studies with a flexible new radiation code. Part I. Choosing a configuration for a large-scale model, *Q. J. R. Meteorol. Soc.*, *122*, 689–719, 1996.
Fouquart, Y., and B. Bonnel, Computation of solar heating of the Earth's atmosphere. A new parameterization, *Beitr. Phys. Atmos.*, *53*, 35–61, 1980.
Ghan, S. J., C. C. Chuang, and J. E. Penner, A parameterization of cloud droplet nucleation, I, Single aerosol type, *Atmos. Res.*, *30*, 192–221, 1993.
Ghan, S. J., L. R. Leung, R. C. Easter, and H. Abdul-Razzak, Prediction of droplet number in a general circulation model, *J. Geophys. Res.*, *102*, 21,777–21,794, 1997.
Ghan, S. J., L. R. Leung, and J. McCaa, A comparison of three different modeling strategies for evaluating cloud and radiation parameterizations, *Mon. Wea. Rev.*, *127*, 1967–1984, 1999.
Gregory, D., and P. R. Rowntree, A mass flux convection scheme with representation of cloud ensemble characteristics and stability-dependent closure, *Mon. Wea. Rev.*, *118*, 1483–1506, 1990.
Gregory, D., J.-J. Morcrette, C. Jacob, A. C. M. Beljaars, and T. Stockdale, Revision of convection, radiation and cloud schemes in the ECMWF Integrated Forecast System, *Q. J. R. Meteorol. Soc.*, *126*, 1685–1710, 2000.
Guibert, S., J. R. Snider, and J.-L. Brenguier, Aerosol activation in marine stratocumulus clouds Part-I: Measurement validation for a closure study, *J. Geophys. Res.*, *108*(D15), 8628, doi:10.1029/2002JD002678, 2003.
Hallberg, A., et al., Microphysics of clouds: Model versus measurements, *Atmos. Environ.*, *31*, 2453–2462, 1997.
Hansen, J., M. Sato, and R. Ruedy, Radiative forcing and climate response, *J. Geophys. Res.*, *102*, 6831–6864, 1997.
Hansen, J. E., and L. D. Travis, Light scattering in planetary atmospheres, *Space Sci. Rev.*, *16*, 527–610, 1974.
Harshvardhan, S. E. Schwartz, C. M. Benkovitz, and G. Guo, Aerosol influence on cloud microphysics examined by satellite measurements and chemical transport modeling, *J. Atmos. Sci.*, *59*, 714–725, 2002.
Hartke, G. J., and D. Rind, Improved surface and boundary layer models for the Goddard Institute for Space Studies general circulation model, *J. Geophys. Res.*, *102*, 16,407–16,422, 1997.
Jones, A., D. L. Roberts, M. J. Woodage, and C. E. Johnson, Indirect sulphate aerosol forcing in a climate model with an interactive sulphur cycle, *J. Geophys. Res.*, *106*, 20,293–20,310, 2001.
Khairoutdinov, M., and Y. Kogan, A new cloud physics parameterization in a large-eddy simulation model of marine stratocumulus, *Mon. Wea. Rev.*, *128*, 229–243, 2000.
Lacis, A. A., and J. E. Hansen, A parameterization for the absorption of solar radiation in the Earth's atmosphere, *J. Atmos. Sci.*, *31*, 118–133, 1974.

Leaitch, W. R., C. M. Banic, G. A. Isaac, M. D. Couuture, P. S. K. Liu, I. Gultepe, S.-M. Li, L. Kleinman, P. H. Daum, and J. I. MacPherson, Physical and chemical observations in marine stratus during the 1993 North Atlantic Regional Experiment: Factors controlling cloud droplet number concentration, *J. Geophys. Res.*, 101, 29,123–29,135, 1996.

Le Treut, H., and Z.-X. Li, Sensitivity of an atmospheric general circulation model to prescribed SST changes: Feedback effects associated with the simulation of cloud optical properties, *Clim. Dyn.*, 5, 175–187, 1991.

Lin, H., and W. R. Leaitch, Development of an in-cloud aerosol activation parameterization for climate modelling, in: Proceedings of the WMO Workshop on Measurement of Cloud Properties for Forecasts of Weather, Air Quality and Climate. World Meteorol. Organ., Geneva, 328–335, 1997.

Lock, A., The numerical representation of entrainment in parameterizations of boundary layer turbulent mixing, *Mon. Wea. Rev.*, 129, 1148–1163, 2001.

Lohmann, U., Possible aerosol effects on ice clouds via contact nucleation, *J. Atmos. Sci.*, 59, 647–656, 2002.

Lohmann, U., J. Feichter, C. C. Chuang, and J. E. Penner, Predicting the number of cloud droplets in the ECHAM GCM, *J. Geophys. Res.*, 104, 9169–9198, 1999.

Louis, J.-F., A parametric model of vertical eddy fluxes in the atmosphere, *Bound. Layer Meteorol.*, 17, 187–202, 1979.

Manton, M. J., and W. R. Cotton, Formulation of approximate equations for modeling moist deep convection on the mesoscale, Atmos. Sci. Pap. 266, 62 pp., Dep. of Atmos. Sci., Colo. State Univ., Fort Collins, Colo., 1977.

Martin, G. M., D. W. Johnson, and A. Spice, The measurement and parameterisation of effective radius of droplets in warm stratocumulus clouds, *J. Atmos. Sci.*, 51, 1823–1842, 1994.

Menon, S., A. D. Del Genio, D. Koch, and G. Tselioudis, GCM simulations of the aerosol indirect effect: Sensitivity to cloud parameterization and aerosol burden, *J. Atmos. Sci.*, 59, 692–713, 2002.

Mlawer, E. J., S. J. Taubmann, and P. D. Brown, et al., Radiative transfer for inhomogeneous atmospheres: RRTM, a validated correlated-k model for the longwave, *J. Geophys. Res.*, 102, 16,663–16,682, 1997.

Morcrette, J.-J., Radiation and cloud radiative properties in the European Centre for Medium-Range Weather Forecasts forecasting system, *J. Geophys. Res.*, 96, 9121–9132, 1991.

Parol, F., J. Descloitres, and Y. Fouquart, Cloud optical depth and albedo retrievals from bidirectional reflectance measurements of POLDER instruments during ACE-2, *Tellus*, 52B, 888–908, 2000.

Pawlowska, H., and J.-L. Brenguier, Microphysical properties of stratocumulus clouds during ACE-2, *Tellus*, 52B, 868–887, 2000.

Pawlowska, H., and J.-L. Brenguier, An observational study of drizzle formation in stratocumulus clouds during ACE-2 for GCM parameterizations, *J. Geophys. Res.*, 108(D15), 8630, doi:10.1029/2002JD002679, 2003.

Penner, J. E., et al., *Climate Change 2001: The Scientific Basis*, edited by J. T. Houghton et al., pp. 289–348, Cambridge Univ. Press, New York, 2001.

Pincus, R., and S. A. Klein, Unresolved spatial variability and microphysical process rates in large-scale models, *J. Geophys. Res.*, 105, 27,059–27,065, 2000.

Pincus, R., S. A. McFarlane, and S. A. Klein, Albedo bias and the horizontal variability of clouds in subtropical marine boundary layers: Observations from ships and satellites, *J. Geophys. Res.*, 104, 6183–6191, 1999.

Pope, V. D., M. L. Gallani, P. R. Rowntree, and R. A. Stratton, The impact of new physical parameterizations in the Hadley Centre climate model: HadAM3, *Clim. Dyn.*, 16, 123–146, 2000.

Raes, F., T. Bates, F. McGovern, and M. Van Liedekerke, The second aerosol characterization experiment (ACE-2), General context and main results, *Tellus, Ser. B*, 52, 11–126, 2000.

Reynolds, R. W., and T. M. Smith, A high-resolution global sea surface temperature climatology, *J. Clim.*, 8, 1571–1583, 1995.

Roeckner, E., K. Arpe, L. Bengtsson, M. Christoph, M. Claussen, L. Duemenil, M. Esch, M. Giorgetta, U. Schlese, and U. Schulzweida, The atmospheric general circulation model ECHAM-4: Model description and simulation of present-day climate, *MPI Rep. 218*, Max Planck Inst., Hamburg, Germany, 1996.

Rossow, W. B., and R. A. Schiffer, ISCCP cloud data products, *Bull. Am. Meteorol. Soc.*, 72, 2–20, 1991.

Rotstayn, L. D., A physically based scheme for the treatment of stratiform clouds and precipitation in large-scale models. I: Description and evaluation of the microphysical processes, *Q. J. R. Meteorol. Soc.*, 123, 1227–1282, 1997.

Rotstayn, L. D., On the tuning of auto-conversion parameterizations in climate models, *J. Geophys. Res.*, 105, 15,495–15,507, 2000.

Rotstayn, L. D., B. F. Ryan, and J. J. Katzfey, A scheme for calculation of the liquid fraction in mixed-phase stratiform clouds in large-scale models, *Mon. Wea. Rev.*, 128, 1070–1088, 2000.

Schröder, M., R. Bennartz, L. Schüller, R. Preusker, P. Albert, and J. Fischer, Generating cloudmasks in spatial high-resolution observations of clouds using texture and radiance information, *Int. J. Remote Sens.*, 23, 4247–4261, 2002.

Schüller, L., J.-L. Brenguier, and H. Pawlowska, Retrieval of the microphysical, geometrical and radiative properties of marine stratocumulus from remote sensing, *J. Geophys. Res.*, 108(D15), 8631, doi:10.1029/2002JD002680, 2003.

Schwartz, S. E., Harshvardhan, and C. M. Benkovitz, Influence of anthropogenic aerosol on cloud optical depth and albedo shown by satellite measurements and chemical transport modeling, *Proc. Natl. Acad. Sci.*, 99, 1784–1789, 2002.

Schwarzkopf, M. D., and S. B. Fels, The simplified exchange method revisited: An accurate, rapid method for computation of infrared cooling rates and fluxes, *J. Geophys. Res.*, 96, 9075–9096, 1991.

Slingo, A., A GCM parameterization for the shortwave radiative properties of water clouds, *J. Atmos. Sci.*, 46, 1419–1427, 1989.

Smith, R. N. B., A scheme for predicting layer clouds and their water content in a general circulation model, *Q. J. R. Meteorol. Soc.*, 116, 435–460, 1990.

Snider, J. R., S. Guibert, and J.-L. Brenguier, Aerosol activation in marine stratocumulus clouds: 2. Köhler and parcel theory closure studies, *J. Geophys. Res.*, 108(D15), 8629, doi:10.1029/2002JD002692, 2003.

Stevens, B., et al., Dynamics and chemistry of marine stratocumulus DYCOMS-II, *Bull. Am. Meteorol. Soc.*, 84, 579–593, 2003.

Sundqvist, H., E. Berge, and J. E. Kristjansson, Condensation and cloud parameterization studies with a mesoscale numerical weather prediction model, *Mon. Wea. Rev.*, 117, 1641–1657, 1989.

Tompkins, A. M., A prognostic parameterization for the subgrid-scale variability of water vapor and clouds in large-scale models and its use to diagnose cloud cover, *J. Atmos. Sci.*, 59, 1917–1942, 2002.

Tripoli, G. J., and W. R. Cotton, A numerical investigation of several factors contributing to the observed variable intensity of deep convection over South Florida, *J. Appl. Meteorol.*, 19, 1037–1063, 1980.

Twomey, S., The influence of pollution on the shortwave albedo of clouds, *J. Atmos. Sci.*, 34, 1149–1152, 1977.

Verver, G., F. Raes, D. Vogelezand, and D. Johnson, The 2nd aerosol characterization experiment (ACE-2), Meteorological and chemical content, *Tellus, Ser. B*, 52, 126–140, 2000.

Wilson, D. R., and S. P. Ballard, A microphysically based precipitation scheme for the UK Meteorological Office Unified Model, *Q. J. R. Meteorol. Soc.*, 125, 1607–1636, 1999.

Wood, R., P. R. Field, and W. R. Cotton, Auto-conversion rate bias in stratiform boundary layer cloud parameterizations, *J. Atmos. Res.*, 65, 109–128, 2002.

Xie, S. C., et al., Intercomparison and evaluation of GCM cumulus parameterizations under summertime midlatitude continental conditions, *Q. J. R. Meteorol. Soc.*, 128, 1095–1135, 2002.

Zhang, Y., R. C. Easter, S. J. Ghan, and H. Abdul-Razzak, Impact of aerosol size representation on modeling aerosol-cloud interactions, *J. Geophys. Res.*, 107(D21), 4558, doi:10.1029/2001JD001549, 2002.

————————

O. Boucher, Laboratoire d'Optique Atmosphérique, Université des Sciences et Technologies de Lille, F-59655 Villeneuve d'Ascq, France.

J.-L. Brenguier, Météo-France-CNRS, CNRM-GAME, F-31057 Toulouse, France.

P. Davison, Environment Systems Group, ADS, Wolverhampton WV6 8TQ, UK.

A. D. Del Genio and S. Menon, NASA Goddard Institute for Space Studies/Columbia University, New York, NY 10025, USA. (smenon@giss.nasa.gov)

J. Feichter, Max Planck Institute for Meteorology, D-20146 Hamburg, Germany.

S. Ghan, Climate Physics Group, Pacific Northwest National Laboratory, Richland, WA 99352, USA.

S. Guibert, Météo-France-CNRS, CNRM-GAME, F-31057 Toulouse, France.

X. Liu and J. E. Penner, Department of Atmospheric, Oceanic and Space Sciences, University of Michigan, Ann Arbor, MI 48109-2143, USA.

U. Lohmann, Department of Physics and Atmospheric Science, Dalhousie University, Halifax, Canada B3H 3J5.

H. Pawlowska, Instutute of Physics, Warsaw University, 02-093 Warsaw, Poland.

J. Quaas, Laboratoire de Météorologie Dynamique/CNRS, F-75252 Paris, France.

D. L. Roberts, Hadley Centre, Met Office, Exeter EX1 3PB, UK.

L. Schüller, Institut für Weltraumwissenschaften, Freie Universität, Berlin, Germany.

J. Snider, Department of Atmospheric Science, University of Wyoming, Laramie, WY 82071-3038, USA.